Standard Reference Materials:

Preparation and Certification of SRM–2530, Ellipsometric Parameters Δ and ψ and Derived Thickness and Refractive Index of a Silicon Dioxide Layer on Silicon

G. A. Candela, D. Chandler-Horowitz, J. F. Marchiando,
D. B. Novotny, B. J. Belzer, and M. C. Croarkin

National Engineering Laboratory
National Institute of Standards and Technology
Gaithersburg, MD 20899

NOTE: As of 23 August 1988, the National Bureau of Standards (NBS) became the National Institute of Standards and Technology (NIST) when President Reagan signed into law the Omnibus Trade and Competitiveness Act.

U.S. DEPARTMENT OF COMMERCE, C. William Verity, Secretary
NATIONAL INSTITUTE OF STANDARDS AND TECHNOLOGY, Ernest Ambler, Director
(formerly National Bureau of Standards)

Issued October 1988

Library of Congress Catalog Card Number: 88–600591
National Institute of Standards and Technology Special Publication 260-109
Natl. Inst. Stand. Technol. Spec. Publ. 260-109, 48 pages (Oct. 1988)
CODEN: NSPUE2

U.S. GOVERNMENT PRINTING OFFICE
WASHINGTON: 1988

For sale by the Superintendent of Documents, U.S. Government Printing Office, Washington, DC 20402–9325

Preface

Standard Reference Materials (SRM's) as defined by the National Institute of Standards and Technology (NIST), formerly the National Bureau of Standards (NBS), are well-characterized materials, produced in quantity and certified for one or more physical or chemical properties. They are used to assure the accuracy and compatibility of measurements throughout the Nation. SRM's are widely used as primary standards in many diverse fields in science, industry, and technology, both within the United States and throughout the world. They are also used extensively in the fields of environmental and clinical analysis. In many applications, traceability of quality control and measurement processes to the national measurement system is carried out through the mechanism and use of SRM's. For many of the Nation's scientists and technologists, it is therefore of more than passing interest to know the details of the measurements made at NIST in arriving at the certified values of the SRM's produced. An NIST series of papers, of which this publication is a member, called the NIST Special Publication – 260 Series, is reserved for this purpose.

The 260 Series is dedicated to the dissemination of information on different phases of the preparation, measurement, certification, and use of NIST SRM's. In general, much more detail will be found in these papers than is generally allowed, or desirable, in scientific journal articles. This enables the user to assess the validity and accuracy of the measurement processes employed, to judge the statistical analysis, and to learn details of techniques and methods utilized for work entailing greatest care and accuracy. These papers also should provide sufficient additional information not found on the certificate so that new applications in diverse fields not foreseen at the time the SRM was originally issued will be sought and found.

Inquiries concerning the technical content of this paper should be directed to the author(s). Other questions concerned with the availability, delivery, price, and so forth, will receive prompt attention from:

Office of Standard Reference Materials
National Institute of Standards and Technology
Gaithersburg, MD 20899

Stanley D. Rasberry, Chief
Office of Standard Reference Materials

OTHER NIST PUBLICATIONS IN THIS SERIES

Seward, R. W., ed., NBS Standard Reference Materials Catalog 1988-89, NBS Spec. Publ. 260 (January 1988)

Michaelis, R. E., and Wyman, L. L., Standard Reference Materials: Preparation of White Cast Iron Spectrochemical Standards, NBS Misc. Publ. 260-1 (June 1964). COM74-11061**

Michaelis, R. E., Wyman, L. L., and Flitsch, R., Standard Reference Materials: Preparation of NBS Copper-Base Spectrochemical Standards, NBS Misc. Publ. 260-2 (October 1964). COM74-11063**

Michaelis, R. E., Yakowitz, H., and Moore, G. A., Standard Reference Materials: Metallographic Characterization of an NBS Spectrometric Low-Alloy Steel Standard, NBS Misc. Publ. 260-3 (October 1964). COM74-11060**

Alvarez, R., and Flitsch, R., Standard Reference Materials: Accuracy of Solution X-Ray Spectrometric Analysis of Copper-Base Alloys, NBS Misc. Publ. 260-5 (March 1965). PB168068**

Shultz, J. I., Standard Reference Materials: Methods for the Chemical Analysis of White Cast Iron Standards, NBS Misc. Publ. 260-6 (July 1965). COM74-11068**

Bell, R. K., Standard Reference Materials: Methods for the Chemical Analysis of NBS Copper-Base Spectrochemical Standards, NBS Misc. Publ. 260-7 (October 1965). COM74-11067**

Richmond, M. S., Standard Reference Materials: Analysis of Uranium Concentrates at the National Bureau of Standards, NBS Misc. Publ. 260-8 (December 1965). COM74-11066**

Anspach, S. C., Cavallo, L. M., Garfinkel, S. B., Hutchinson, J. M. R., and Smith, C. N., Standard Reference Materials: Half Lives of Materials Used in the Preparation of Standard Reference Materials of Nineteen Radioactive Nuclides Issued by the National Bureau of Standards, NBS Misc. Publ. 260-9 (November 1965). COM74-11065**

Yakowitz, H., Vieth, D. L., Heinrich, K. F. J., and Michaelis, R. E., Standard Reference Materials: Homogeneity Characterization of NBS Spectrometric Standards II: Cartridge Brass and Low-Alloy Steel, NBS Misc. Publ. 260-10 (December 1965). COM74-11064**

Napolitano, A., and Hawkins, E. G., Standard Reference Materials: Viscosity of Standard Lead-Silica Glass, NBS Misc. Publ. 260-11 (November 1966).

Yakowitz, H., Vieth, D. L., and Michaelis, R. E., Stanc ard Reference Materials: Homogeneity Characteriz tion of NBS Spectrometric Standards III: White Ca Iron and Stainless Steel Powder Compact, NBS Mis Publ. 260-12 (September 1966).

Menis, O., and Sterling, J. T., Standard Referenc Materials: Determination of Oxygen in Ferrou Materials—SRM 1090, 1091, and 1092, NBS Mis Publ. 260-14 (September 1966).

Yakowitz, H., Michaelis, R. E., and Vieth, D. L., Stanc ard Reference Materials: Homogeneity Characteriz tion of NBS Spectrometric Standards IV: Preparatic and Microprobe Characterization of W-20% M Alloy Fabricated by Powder Metallurgical Method NBS Spec. Publ. 260-16 (January 1969). COM7 11062**

Paule, R. C., and Mandel, J., Standard Referenc Materials: Analysis of Interlaboratory Measuremen on the Vapor Pressure of Gold (Certification of Stanc ard Reference Material 745). NBS Spec. Publ. 260-1 (January 1970). PB190071**

Paule, R. C., and Mandel, J., Standard Referenc Materials: Analysis of Interlaboratory Measuremen on the Vapor Pressures of Cadmium and Silver, NB Spec. Publ. 260-21 (January 1971). COM74-11359*

Yakowitz, H., Fiori, C. E., and Michaelis, R. E., Stan ard Reference Materials: Homogeneity Characteriz tion of Fe-3 Si Alloy, NBS Spec. Publ. 260-2 (February 1971). COM74-11357**

Napolitano, A., and Hawkins, E. G., Standard Referen Materials: Viscosity of a Standard Borosilicate Glas NBS Spec. Publ. 260-23 (December 1970). COM7 00157**

Sappenfield, K. M., Marinenko, G., and Hague, J. I Standard Reference Materials: Comparison of Red Standards, NBS Spec. Publ. 260-24 (January 197 COM72-50058**

Hicho, G. E., Yakowitz, H., Rasberry, S. D., a Michaelis, R. E., Standard Reference Materials: Standard Reference Material Containing Nominal Four Percent Austenite, NBS Spec. Publ. 260- (February 1971). COM74-11356**

Martin, J. F., Standard Reference Materials: Natior Bureau of Standards-US Steel Corporation Joi Program for Determining Oxygen and Nitrogen Steel, NBS Spec. Publ. 260-26 (February 1971). I 81176620**

Garner, E. L., Machlan, L. A., and Shields, W. R., Standard Reference Materials: Uranium Isotopic Standard Reference Materials, NBS Spec. Publ. 260-27 (April 1971). COM74-11358**

Heinrich, K. F. J., Myklebust, R. L., Rasberry, S. D., and Michaelis, R. E., Standard Reference Materials: Preparation and Evaluation of SRM's 481 and 482 Gold-Silver and Gold-Copper Alloys for Microanalysis, NBS Spec. Publ. 260-28 (August 1971). COM71-50365**

Geller, S. B., Standard Reference Materials: Calibration of NBS Secondary Standard Magnetic Tape (Computer Amplitude Reference) Using the Reference Tape Amplitude Measurement "Process A-Model 2," NBS Spec. Publ. 260-29 (June 1971). COM71-50282**

Gorozhanina, R. S., Freedman, A. Y., and Shaievitch, A. B. (translated by M. C. Selby), Standard Reference Materials: Standard Samples Issued in the USSR (A Translation from the Russian), NBS Spec. Publ. 260-30 (June 1971). COM71-50283**

Hust, J. G., and Sparks, L. L., Standard Reference Materials: Thermal Conductivity of Electrolytic Iron SRM 734 from 4 to 300 K, NBS Spec. Publ. 260-31 (November 1971). COM71-50563**

Mavrodineanu, R., and Lazar, J. W., Standard Reference Materials: Standard Quartz Cuvettes for High Accuracy Spectrophotometry, NBS Spec. Publ. 260-32 (December 1973). COM74-50018**

Wagner, H. L., Standard Reference Materials: Comparison of Original and Supplemental SRM 705, Narrow Molecular Weight Distribution Polystyrene, NBS Spec. Publ. 260-33 (May 1972). COM72-50526**

Sparks, L. L., and Hust, J. G., Standard Reference Materials: Thermal Conductivity of Austenitic Stainless Steel, SRM 735 from 5 to 280 K, NBS Spec. Publ. 260-35 (April 1972.) COM72-50368**

Cali, J. P., Mandel, J., Moore, L. J., and Young, D. S., Standard Reference Materials: A Referee Method for the Determination of Calcium in Serum NBS SRM 915, NBS Spec. Publ. 260-36 (May 1972). COM72-50527**

Shultz, J. I., Bell, R. K., Rains, T. C., and Menis, O., Standard Reference Materials: Methods of Analysis of NBS Clay Standards, NBS Spec. Publ. 260-37 (June 1972). COM72-50692**

Clark, A. F., Denson, V. A., Hust, J. G., and Powell, R. L., Standard Reference Materials: The Eddy Current Decay Method for Resistivity Characterization of High-Purity Metals, NBS Spec. Publ. 260-39 (May 1972). COM72-50529**

McAdie, H. G., Garn, P. D., and Menis, O., Standard Reference Materials: Selection of Thermal Analysis Temperature Standards Through a Cooperative Study (SRM 758, 759, 760), NBS Spec. Publ. 260-40 (August 1972) COM72-50776**

Wagner, H. L., and Verdier, P. H., eds., Standard Reference Materials: The Characterization of Linear Polyethylene, SRM 1475, NBS Spec. Publ. 260-42 (September 1972). COM72-50944**

Yakowitz, H., Ruff, A. W., and Michaelis, R. E., Standard Reference Materials: Preparation and Homogeneity Characterization of an Austenitic Iron-Chromium-Nickel Alloy, NBS Spec. Publ. 260-43 (November 1972). COM73-50760**

Schooley, J. F., Soulen, R. J., Jr., and Evans, G. A., Jr., Standard Reference Materials: Preparation and Use of Superconductive Fixed Point Devices, SRM 767, NBS Spec. Publ. 260-44 (December 1972). COM73-50037**

Greifer, B., Maienthal, E. J., Rains, T. C., and Rasberry, S. D., Standard Reference Materials: Powdered Lead-Based Paint, SRM 1579, NBS Spec. Publ. 260-45 (March 1973). COM73-50226**

Hust, J. G., and Giarratano, P. J., Standard Reference Materials: Thermal Conductivity and Electrical Resistivity Standard Reference Materials: Austenitic Stainless Steel, SRM's 735 and 798, from 4 to 1200 K, NBS Spec. Publ. 260-46 (March 1975). COM75-10339**

Hust, J. G., Standard Reference Materials: Electrical Resistivity of Electrolytic Iron, SRM 797, and Austenitic Stainless Steel, SRM 798, from 5 to 280 K, NBS Spec. Publ. 260-47 (February 1974). COM74-50176**

Mangum, B. W., and Wise, J. A., Standard Reference Materials: Description and Use of Precision Thermometers for the Clinical Laboratory, SRM 933 and SRM 934, NBS Spec. Publ. 260-48 (May 1974). COM74-50533**

Carpenter, B. S., and Reimer, G. M., Standard Reference Materials: Calibrated Glass Standards for Fission Track Use, NBS Spec. Publ. 260-49 (November 1974). COM74-51185**

Hust, J. G., and Giarratano, P. J., Standard Reference Materials: Thermal Conductivity and Electrical Resistivity Standard Reference Materials: Electrolytic Iron, SRM's 734 and 797 from 4 to 1000 K, NBS Spec. Publ. 260-50 (June 1975). COM75-10698**

Mavrodineanu, R., and Baldwin, J. R., Standard Reference Materials: Glass Filters As a Standard Reference Material for Spectrophotometry-Selection, Preparation, Certification, Use-SRM 930 NBS Spec. Publ. 260-51 (November 1975). COM75-10339**

Hust, J. G., and Giarratano, P. J., Standard Reference Materials: Thermal Conductivity and Electrical Resistivity Standard Reference Materials 730 and 799, from 4 to 3000 K, NBS Spec. Publ. 260-52 (September 1975). COM75-11193**

Durst, R. A., Standard Reference Materials: Standardization of pH Measurements, NBS Spec. Publ. 260-53 (February 1988, Revision of December 1975 version).

Burke, R. W., and Mavrodineanu, R., Standard Reference Materials: Certification and Use of Acidic Potassium Dichromate Solutions as an Ultraviolet Absorbance Standard, NBS Spec. Publ. 260-54 (August 1977). PB272168**

Ditmars, D. A., Cezairliyan, A., Ishihara, S., and Douglas, T. B., Standard Reference Materials: Enthalpy and Heat Capacity; Molybdenum SRM 781, from 273 to 2800 K, NBS Spec. Publ. 260-55 (September 1977). PB272127**

Powell, R. L., Sparks, L. L., and Hust, J. G., Standard Reference Materials: Standard Thermocouple Material, Pt-67: SRM 1967, NBS Spec. Publ. 260-56 (February 1978). PB277172**

Barnes, J. D., and Martin, G. M., Standard Reference Materials: Polyester Film for Oxygen Gas Transmission Measurements SRM 1470, NBS Spec. Publ. 260-58 (June 1979). PB297098**

Velapoldi, R. A., Paule, R. C., Schaffer, R., Mandel, J., and Moody, J. R., Standard Reference Materials: A Reference Method for the Determination of Sodium in Serum, NBS Spec. Publ. 260-60 (August 1978). PB286944**

Verdier, P H., and Wagner, H. L., Standard Reference Materials: The Characterization of Linear Polyethylene (SRM 1482, 1483, 1484), NBS Spec. Publ. 260-61 (December 1978). PB289899**

Soulen, R. J., and Dove, R. B., Standard Reference Materials: Temperature Reference Standard for Use Below 0.5 K (SRM 768), NBS Spec. Publ. 260-62 (April 1979). PB294245**

Velapoldi, R. A., Paule, R. C., Schaffer, R., Mandel, J., Machlan, L. A., and Gramlich, J. W., Standard Reference Materials: A Reference Method for the Determination of Potassium in Serum, NBS Spec. Publ. 260-63 (May 1979). PB297207**

Velapoldi, R. A., and Mielenz, K. D., Standard Reference Materials: A Fluorescence Standard Reference Material Quinine Sulfate Dihydrate (SRM 936), NBS Spec. Publ. 260-64 (January 1980). PB80-132046**

Marinenko, R. B., Heinrich, K. F. J., and Ruegg, F. C., Standard Reference Materials: Micro-Homogeneity Studies of NBS Standard Reference Materials, NBS Research Materials, and Other Related Samples, NBS Spec. Publ. 260-65 (September 1979). PB300461**

Venable, W. H., Jr., and Eckerle, K. L., Standard Reference Materials: Didymium Glass Filters for Calibrating the Wavelength Scale of Spectrophotometers-SRM 2009, 2010, 2013, and 2014, NBS Spec. Publ. 260-66 (October 1979). PB80-104961**

Velapoldi, R. A., Paule, R. C., Schaffer, R., Mandel, J., Murphy, T. J., and Gramlich, J. W., Standard Reference Materials: A Reference Method for the Determination of Chloride in Serum, NBS Spec. Publ. 260-67 (November 1979). PB80-110117**

Mavrodineanu, R., and Baldwin, J. R., Standard Reference Materials: Metal-On-Quartz Filters as a Standard Reference Material for Spectrophotometry SRM 2031, NBS Spec. Publ. 260-68 (April 1980). PB80-197486**

Velapoldi, R. A., Paule, R. C., Schaffer, R., Mandel, J., Machlan, L. A., Garner, E. L., and Rains, T. C., Standard Reference Materials: A Reference Method for the Determination of Lithium in Serum, NBS Spec. Publ. 260-69 (July 1980). PB80-209117**

Marinenko, R. B., Biancaniello, F., Boyer, P. A., Ruff, A. W., and DeRobertis, L., Standard Reference Materials: Preparation and Characterization of an Iron-Chromium-Nickel Alloy for Microanalysis, NBS Spec. Publ. 260-70 (May 1981). PB84-165349**

Seward, R. W., and Mavrodineanu, R., Standard Reference Materials: Summary of the Clinical Laboratory Standards Issued by the National Bureau of Standards, NBS Spec. Publ. 260-71 (November 1981). PB82-135161**

Reeder, D. J., Coxon, B., Enagonio, D., Christensen, R. G., Schaffer, R., Howell, B. F., Paule, R. C., and Mandel, J., Standard Reference Materials: SRM 900, Antiepilepsy Drug Level Assay Standard, NBS Spec. Publ. 260-72 (June 1981). PB81-220758

Interrante, C. G., and Hicho, G. E., Standard Reference Materials: A Standard Reference Material Containing Nominally Fifteen Percent Austenite (SRM 486), NBS Spec. Publ. 260-73 (January 1982). PB82-215559**

Marinenko, R. B., Standard Reference Materials: Preparation and Characterization of K-411 and K-414 Mineral Glasses for Microanalysis: SRM 470, NBS Spec. Publ. 260-74 (April 1982). PB82-221300**

Weidner, V. R., and Hsia, J. J., Standard Reference Materials: Preparation and Calibration of First Surface Aluminum Mirror Specular Reflectance Standards (SRM 2003a), NBS Spec. Publ. 260-75 (May 1982). PB82-221367**

Hicho, G. E., and Eaton, E. E., Standard Reference Materials: A Standard Reference Material Containing Nominally Five Percent Austenite (SRM 485a), NBS Spec. Publ. 260-76 (August 1982). PB83-115568**

Furukawa, G. T., Riddle, J. L., Bigge, W. G., and Pfieffer, E. R., Standard Reference Materials: Application of Some Metal SRM's as Thermometric Fixed Points, NBS Spec. Publ. 260-77 (August 1982). PB83-117325**

Hicho, G. E., and Eaton, E. E., Standard Reference Materials: Standard Reference Material Containing Nominally Thirty Percent Austenite (SRM 487), NBS Spec. Publ. 260-78 (September 1982). PB83-115576**

Richmond, J. C., Hsia, J. J., Weidner, V. R., and Wilmering, D. B., Standard Reference Materials: Second Surface Mirror Standards of Specular Spectral Reflectance (SRM's 2023, 2024, 2025), NBS Spec. Publ. 260-79 (October 1982). PB84-203447**

Schaffer, R., Mandel, J., Sun, T., Cohen, A., and Hertz, H. S., Standard Reference Materials: Evaluation by an ID/MS Method of the AACC Reference Method for Serum Glucose, NBS Spec. Publ. 260-80 (October 1982). PB84-216894**

Burke, R. W., and Mavrodineanu, R., Standard Reference Materials: Accuracy in Analytical Spectrophotometry, NBS Spec. Publ. 260-81 (April 1983). PB83-214536**

Weidner, V. R., Standard Reference Materials: White Opal Glass Diffuse Spectral Reflectance Standards for the Visible Spectrum (SRM's 2015 and 2016), NBS Spec. Publ. 260-82 (April 1983). PB83-220723**

Bowers, G. N., Jr., Alvarez, R., Cali, J. P., Eberhardt, K. R., Reeder, D. J., Schaffer, R., and Uriano, G. A., Standard Reference Materials: The Measurement of the Catalytic (Activity) Concentration of Seven Enzymes in NBS Human Serum SRM 909, NBS Spec. Publ. 260-83 (June 1983). PB83-239509**

Gills, T. E., Seward, R. W., Collins, R. J., and Webster, W. C., Standard Reference Materials: Sampling, Materials Handling, Processing, and Packaging of NBS Sulfur in Coal Standard Reference Materials 2682, 2683, 2684, and 2685, NBS Spec. Publ. 260-84 (August 1983). PB84-109552**

Swyt, D. A., Standard Reference Materials: A Look at Techniques for the Dimensional Calibration of Standard Microscopic Particles, NBS Spec. Publ. 260-85 (September 1983). PB84-112648**

Hicho, G. E., and Eaton, E. E., Standard Reference Materials: A Standard Reference Material Containing Two and One-Half Percent Austenite, SRM 488, NBS Spec. Publ. 260-86 (December 1983). PB84-143296**

Mangum, B. W., Standard Reference Materials: SRM 1969: Rubidium Triple-Point - A Temperature Reference Standard Near 39.30 °C, NBS Spec. Publ. 260-87 (December 1983). PB84-149996**

Gladney, E. S., Burns, C. E., Perrin, D. R., Roelandts, I., and Gills, T. E., Standard Reference Materials: 1982 Compilation of Elemental Concentration Data for NBS Biological, Geological, and Environmental Standard Reference Materials, NBS Spec. Publ. 260-88 (March 1984). PB84-218338**

Hust, J. G., Standard Reference Materials: A Fine-Grained, Isotropic Graphite for Use as NBS Thermophysical Property RM's from 5 to 2500 K, NBS Spec. Publ. 260-89 (September 1984). PB85-112886**

Hust, J. G., and Lankford, A. B., Standard Reference Materials: Update of Thermal Conductivity and Electrical Resistivity of Eleetrolytic Iron, Tungsten, and Stainless Steel, NBS Spec. Publ. 260-90 (September 1984). PB85-115814**

Goodrich, L. F., Vecchia, D. F., Pittman, E. S., Ekin, J. W., and Clark, A. F., Standard Reference Materials: Critical Current Measurements on an NbTi Superconducting Wire Standard Reference Material, NBS Spec. Publ. 260-91 (September 1984). PB85-118594**

Carpenter, B. S., Standard Reference Materials: Calibrated Glass Standards for Fission Track Use (Supplement to NBS Spec. Publ. 260-49), NBS Spec. Publ. 260-92 (September 1984). PB85-113025**

Ehrstein, J.R., Standard Reference Materials: Preparation and Certification of Standard Reference Materials for Calibration of Spreading Resistance Probes, NBS Spec. Publ. 260-93 (January 1985). PB85-177921**

Gills, T. E., Koch, W. F., Stolz, J. W., Kelly, W. R., Paulsen, P. J., Colbert, J. C., Kirklin, D. R., Pei, P.T.S., Weeks, S., Lindstrom, R. M., Fleming, R. F., Greenberg, R. R., and Paule, R. C., Standard Reference Materials: Methods and Procedures Used at the National Bureau of Standards to Certify Sulfur in Coal SRM's for Sulfur Content, Calorific Value, Ash Content, NBS Spec. Publ. 260-94 (December 1984). PB85-165900**

Mulholland, G. W., Hartman, A. W., Hembree, G. G., Marx, E., and Lettieri, T. R., Standard Reference Materials: Development of a 1 μm Diameter Particle Size Standard, SRM 1690, NBS Spec. Publ. 260-95 (May 1985). SN003-003-02665-4*

Carpenter, B. S., Gramlich, J. W., Greenberg, R. R., Machlan, L. A., DeBievre, P., Eschbach, H. L., Meyer, H., Van Audenhove, J., Connolly, V. E., Trahey, N. M., and Zook, A. C., Standard Reference Materials: Uranium-235 Isotopic Abundance Standard Reference Materials for Gamma Spectrometry Measurements, NBS Spec. Publ. 260-96 (September 1986). PB87-108544**

Mavrodineanu, R., and Gills, T. E., Standard Reference Materials: Summary of the Coal, Ore, Mineral, Rock, and Refactory Standards Issued by the National Bureau of Standards, NBS Spec. Publ. 260-97 (September 1985). SN003-003-02688-3*

Hust, J. G., Standard Reference Materials: Glass Fiberboard SRM for Thermal Resistance, NBS Spec. Publ. 260-98 (August 1985). SN003-003-02674-3*

Callanan, J. E., Sullivan, S. A., and Vecchia, D. F., Standard Reference Materials: Feasibility Study for the Development of Standards Using Differential Scanning Calorimetry, NBS Spec. Publ. 260-99 (August 1985). SN003-003-02675-1*

Taylor, J. K., Standard Reference Materials: Handbook for SRM Users, NBS Spec. Publ. 260-100 (September 1985). PB86-110897**

Mangum, B. W., Standard Reference Materials: SRM 1970, Succinonitrile Triple-Point Standard: A Temperature Reference Standard Near 58.08 °C, NBS Spec. Publ. 260-101 (March 1986). SN003-003-02722-7*

Weidner, V. R., Mavrodineanu, R., Mielenz, K. D., Velapoldi, R. A., Eckerle, K. L., and Adams, B., Standard Reference Materials: Holmium Oxide Solution Wavelength Standard from 240 to 640 nm - SRM 2034, NBS Spec. Publ. 260-102 (July 1986). PB86-245727**

Hust, J. G., Standard Reference Materials: Glass Fiberblanket SRM for Thermal Resistance, NBS Spec. Publ. 260-103 (September 1985). SN003-003-02687-5*

Mavrodineanu, R., and Alvarez, R., Standard Reference Materials: Summary of the Biological and Botanical Standards Issued by the National Bureau of Standards, NBS Spec. Publ. 260-104 (November 1985). SN003-003-02704-9*

Mavrodineanu, R., and Rasberry, S. D., Standard Reference Materials: Summary of the Environmental Research, Analysis, and Control Standards Issued by the National Bureau of Standards, NBS Spec. Publ. 260-105 (March 1986). SN003-003-02725-1*

Koch, W. F., ed., Standard Reference Materials: Methods and Procedures Used at the National Bureau of Standards to Prepare, Analyze, and Certify SRM 2694, Simulated Rainwater, and Recommendations for Use, NBS Spec. Publ. 260-106 (July 1986). PB86-247483**

Hartman, A. W., and McKenzie, R. L., Standard Reference Materials: SRM 1965, Microsphere Slide (10 μm Polystyrene Spheres), NBS Spec. Publ. 260-107 (In Preparation).

Mavrodineanu, R., and Gills, T. E., Standard Reference Materials: Summary of Gas Cylinder and Permeation Tube Standard Reference Materials Issued by the National Bureau of Standards, NBS Spec. Publ. 260-108 (May 1987).

Candela, G. A., Chandler-Horowitz, D., Novotny, D. B., Marchiando, J. F., and Belzer, B. J., Standard Reference Materials: Preparation and Certification of an Ellipsometrically Derived Thickness and Refractive Index Standard of a Silicon Dioxide Film (SRM 2530), NIST Spec. Publ. 260-109 (October 1988).

Kirby, R. K., and Kanare, H. M., Standard Reference Materials: Portland Cement Chemical Composition Standards (Blending, Packaging, and Testing), NBS Spec. Publ. 260-110 (February 1988).

Gladney, E. S., O'Malley, B. T., Roelandts, I., and Gills, T. E., Standard Reference Materials: Compilation of Elemental Concentration Data for NBS Clinical, Biological, Geological, and Environmental Standard Reference Materials, NBS Spec. Publ. 260-111 (November 1987).

*Send order with remittance to Superintendent of Documents, U.S. Government Printing Office, Washington, DC 20102. Remittance from foreign countries should include an additional one fourth of the purchase price for postage.

**May be ordered from: National Technical Information Services (NTIS), Springfield, VA 22161.

TABLE OF CONTENTS

Page

Abstract 1

I. Introduction 2

II. Design and Fabrication of SRM-2530 3

III. Ellipsometric Theory 4

IV. Sources of Instrumental Uncertainties 6

V. Analysis of the Fourier Coefficients 9

VI. Uncertainties in the Ellipsometric Parameters 11

VII. Description of the Least-Squares Analysis 13

VIII. Parameters of the Two-Layer Model 13

IX. Sensitivity Analysis and Uncertainties in the Model Parameters 15

X. Parameters of the One-Layer Model 15

XI. Goodness-of-Fit Test 16

XII. Computer Program for Determining the Thickness of the SRM Silicon Dioxide Layer 17

Acknowledgments 17

References 17

Appendix 1. Ellipsometer Precision and Uncertainty 21

Appendix 2. Formulation of the Least-Squares Problem 26

Appendix 3. Sensitivity Analysis of the Model Parameters 31

Appendix 4. Goodness of Fit 34

Appendix 5. Computer Program for Determining the Thickness of the SRM Silicon Dioxide Layer 36

LIST OF TABLES

Page

I. Instrumental Components of Uncertainty 9

II. Short- and Long-Term Precision in the Fourier Coefficients 10

III. Systematic and Random Contributions to the Uncertainties in Δ' and ψ' 12

IV. Parameters and Uncertainties for the Two-Layer Model 14

LIST OF FIGURES

1. Schematic of SRM-2530 19

2. Schematic of Two-Layer Model 20

PREPARATION AND CERTIFICATION OF SRM-2530, ELLIPSOMETRIC PARAMETERS Δ AND ψ AND DERIVED THICKNESS AND REFRACTIVE INDEX OF A SILICON DIOXIDE LAYER ON SILICON

G.A. Candela, D. Chandler-Horowitz, J.F. Marchiando,
D.B. Novotny, and B.J. Belzer
Semiconductor Electronics Division

M.C. Croarkin
Statistical Engineering Division

National Institute of Standards and Technology
(formerly the National Bureau of Standards)
Gaithersburg, Maryland 20899

Abstract

A Standard Reference Material, SRM-2530, has been designed, fabricated, and certified for the ellipsometric parameters delta, Δ, and psi, ψ, and for the derived thickness and refractive index of a silicon dioxide layer on silicon using a highly accurate ellipsometer built at NIST. This SRM is issued primarily to evaluate the accuracy of ellipsometers. The SRM consists of a 76-mm (3-in.) diameter silicon wafer with a silicon dioxide layer of one of three uniform thicknesses, 50, 100, or 200 nm. The design and fabrication of the SRM are presented along with the ellipsometric technique and data analysis leading to certification of this SRM. A least-squares method minimizing the sum of squares of deviations in Δ and ψ between the measured values and those calculated from a model has been used in certifying the SRM. The derived values of the thickness and refractive index may be determined by using either a two-layer or a one-layer model. The two-layer model assumes a silicon dioxide layer on a thin interlayer atop the silicon substrate, whereas the one-layer model assumes a single dielectric layer for the silicon dioxide without the interlayer. The two-layer modeling analysis gives better agreement to the collective multiple sample ellipsometric measurement data than does the one-layer modeling analysis, and gives a value for the refractive index of the silicon dioxide layer that is independent of thickness. Therefore, the certified values of thickness and refractive index are based on the two-layer model.

Key words: ellipsometric parameters; layer refractive index; layer thickness; modeling; silicon dioxide layer; silicon substrate; Standard Reference Materials.

I. Introduction

A computer-controlled variable-angle-of-incidence spectroscopic ellipsometer of high accuracy has been designed and constructed at NIST. This ellipsometer can be used in the following modes of operation: conventional null, principal angle of incidence, and rotating analyzer. The instrument is primarily used for the metrology of semiconductor materials, the calibration of reference standards, and for research projects investigating multiple-layered structures. Further details regarding the ellipsometer may be found in reference 1.

One of the methods for transferring the capabilities of this instrument to the semiconductor industry is to use this ellipsometer to certify the measured ellipsometric quantities, Δ and ψ, and the derived silicon dioxide layer thickness and refractive index of Standard Reference Materials (SRM's) [2,3]. The SRM can be used as an aid in the calibration and the evaluation of optical and mechanical thickness-monitoring instruments as well as ellipsometers for which it was specifically designed [2,4].

The first batch of SRM-2530's consists of approximately 52 wafers in three thickness categories. The thickness categories of 50, 100, and 200 nm refer to the nominal thicknesses of silicon dioxide layers atop silicon substrates. This publication describes the design and fabrication of the SRM's and the ellipsometric and statistical methods for their certification.

Section II describes the design and fabrication of the SRM. Section III, on ellipsometric theory, defines the two ellipsometrically measured quantities, Δ and ψ, that are certified at the principal angle of incidence using the photometric method of ellipsometry with a rotating analyzer. Sources of instrumental uncertainties are assessed in section IV, and the analysis of the precision in the Fourier coefficients that describe the periodically varying light intensity is presented in section V. Table I and Table II summarize these results. Section VI and Table III show how the total uncertainties in Δ and ψ are derived from systematic and random uncertainties.

Section VII discusses the least-squares procedure used to determine the best values of the specimen model parameters. In section VIII, the least-squares procedure is used to analyze the two-layered structure, consisting of a silicon dioxide layer on top of a thin transition layer on silicon [5-7]. Section IX uses the sensitivity analysis to compute the uncertainties in the model parameters. Table IV shows the values for the model parameters found from the measurements and their uncertainties as they would appear on the certificate for a typical SRM at each of three different silicon dioxide layer thicknesses. In section X, a one-layer model, where there is no transition interlayer and each thickness group of SRM is allowed to have a different layer refractive index, is presented and used to compute the corresponding layer thicknesses. In section XI, a goodness-of-fit test is used to compare the two models. In section XII and Appendix 5, a computer program for ellipsometric calculations is described. This program can be used to calculate the layer thicknesses for the one- and two-layer models based on certified Δ and ψ values.

II. Design and Fabrication of SRM-2530

Silicon dioxide on silicon is one of the better characterized layered structures, both chemically and physically. Thermally grown silicon dioxide layers on silicon substrates are stable and easy to clean, and extensive studies exist of the optical properties [8] for both the layer and bulk substrate material. These silicon dioxide layers are the most widely used and measured layers in the semiconductor industry. The SRM was designed to help fulfill a metrological need of the semiconductor industry concerning the thickness and refractive index of silicon dioxide layers.

Design of SRM

The SRM design consists of a 76-mm (3-in.) diameter silicon wafer with a silicon dioxide layer of uniform thickness in the shape of a rectangle, 2.5 cm by 6 cm. Four long, narrow (8 mm by 0.5 mm) rectangular windows were etched through the dioxide layer, and a chromium overlayer was deposited such that its shape bisects the silicon dioxide layer into two approximately equal areas (see Fig. 1) to be used for the ellipsometric measurements. The windows in the silicon dioxide are approximately half covered by the chromium pattern. The patterns of the windows under the chromium can be used for interferometric and stylus profilometric measurements [2]. The chromium overlayer surface can be useful in aligning the ellipsometer components.

Silicon Wafers

High-quality silicon wafers from the same crystal were used for the fabrication of each batch of SRM's. The silicon material is boron-doped, p-type, (100) surface, 3 to 10 ohm-cm resistivity. These wafers were ground flat on the back side and ground flat and polished on the front side. The surface flatness was determined by using a Tropel* wafer flatness tester. The flatness was found to be within one-quarter wavelength of light at the 632.8-nm helium-neon laser line over the measurement spot size of 3- to 10-mm diameter on the wafer.

---

* Certain commercial equipment, instruments, or materials are identified in this paper to adequately specify the experimental procedure. Such identification does not imply recommendation or endorsement by the National Institute of Standards and Technology, nor does it imply that the materials or equipment identified are necessarily the best available for the purpose.

Fabrication of SRM

The silicon dioxide was grown at a temperature of 1050°C in a dry oxygen atmosphe The time of growth was varied to obtain the three thicknesses of 50, 100, and 200 n The uniformity of this dioxide layer thickness was measured using a commercial reflectan spectrometer, and only wafers whose dioxide thicknesses were uniform, varying by less th 0.6 nm over both of the rectangular areas of the silicon dioxide, were used for SRM's. photolithographic technique using a photoresist coating deposited on the dioxide and e etchant of buffered hydrofluoric acid was used to pattern the desired rectangular dioxi and window areas. The photoresist was then removed with acetone, and the wafers washe with deionized water and soaked for 15 minutes in hot concentrated sulfuric acid containi freshly dissolved ammonium persulfate. After this treatment, the wafers were washed i deionized water and spun dry.

In preparation for chromium deposition, the wafer was immersed briefly in 2% hydrofl oric acid to remove the native oxide from the bare silicon areas. A layer of chromiu approximately 150 nm thick was sputtered over the entire wafer surface. The chromiu was then patterned and etched with Cyantek CR-9*. The patterning resulted in leavin approximately half of each of the windows covered with chromium as is shown in Figu 1. All ellipsometric measurements were made on the two areas designated in Figure 1 a left side and right side. The areas are approximately 2.5 cm by 2.5 cm located 0.5 cm t the left and right of the chromium overlayer.

Cleaning of SRM's

Even when the SRM's are stored in clean containers, a contaminating film forms on th surface of the silicon dioxide. This unwanted film forms rapidly, usually 0.1 or 0.2 nm pe week [3], and is removed before measurements are made by rinsing the SRM with reagen grade ethanol and then with deionized water. Each solvent is blown off the wafer surfac with clean nitrogen. The sample is then permitted to stabilize in the atmosphere for 20 t 30 minutes before measurements are made.

III. Ellipsometric Theory

The Fresnel complex amplitude reflection coefficients are

$$R_p = \frac{E_{rp}}{E_{ip}} = |R_p| e^{i\Delta p}, \tag{1}$$

$$R_s = \frac{E_{rs}}{E_{is}} = |R_s| e^{i\Delta s}, \tag{2}$$

where R_p and R_s are the ratios of the reflected electric field vector amplitudes, E_{rp} or E_{rs}, to the incident electric field amplitudes, E_{ip} or E_{is}, for light polarized either parallel, p, or perpendicular, s, to the plane of incidence. The phase shifts of the electric field induced upon reflection are Δ_p and Δ_s, for light polarized parallel and perpendicular to the plane of incidence, respectively. The ellipsometric parameters ψ and Δ are defined by the ratio of R_p to R_s [9]:

$$\frac{R_p}{R_s} = \tan\psi \; e^{i\Delta}, \tag{3}$$

where

$$\Delta = \Delta_p - \Delta_s, \tag{4}$$

$$\tan\psi = \frac{|R_p|}{|R_s|}. \tag{5}$$

In the rotating analyzer ellipsometric (RAE) method which was used to certify the SRM's, monochromatic coherent light passes through a polarizer and onto the sample surface at a given angle of incidence. In this photometric method, the reflected beam goes through a rotating analyzer and the light intensity is measured by a silicon photodiode detector. The light intensity, I, as a function of time, is [10,11] (eq. (A1.1)):

$$I(t) = I_0\big(1 + \alpha\cos 2A(t) + \beta\sin 2A(t)\big), \tag{6}$$

where I_0 is the average intensity and $A(t)$ is the rotating analyzer azimuth. The Fourier coefficients, α and β, are given by

$$\alpha = \frac{\tan^2\psi - \tan^2 P}{\tan^2\psi + \tan^2 P} \tag{7}$$

$$\beta = \frac{2\tan\psi\tan P\cos\Delta}{\tan^2\psi + \tan^2 P}, \tag{8}$$

where P is the measured value of the polarizer azimuth with respect to the plane of incidence.

The Fourier coefficients, α and β, are obtained from a discrete Fourier transform of the measured light intensity as a function of time. Knowing P and the values of α and β, both Δ and ψ may be calculated from the following expressions ((eqs. (A1.3), (A1.4)):

$$\psi = \tan^{-1}\left[\sqrt{\frac{1+\alpha}{1-\alpha}}\,\left|\tan P\right|\right], \qquad 0 \le \psi \le 90°, \tag{9}$$

$$\Delta = \pm\cos^{-1}\left[\sqrt{\frac{\beta^2}{1-\alpha^2}}\right], \qquad -180°<\Delta \le 180°. \tag{10}$$

The sign of Δ must be determined by a separate procedure such as inserting an optical element of known phase retardation between the sample and rotating analyzer [11].

IV. Sources of Instrumental Uncertainties

This section discusses the various uncertainties arising from the components of the ellipsometer. Estimates are made of the uncertainties in the wavelength, $\delta\lambda$; in the angle of incidence, $\delta\phi$; in the polarizer and analyzer azimuths, δP and δA; of effects due to polarizer ellipticity; and of effects due to detector nonlinearity. These systematic and random components of instrumental uncertainties are listed in Table I and are used in section VI to estimate the total uncertainty in the measurement of Δ and ψ.

Wavelength Uncertainty, $\delta\lambda$

A helium-neon laser source is used for both sample alignment and the ellipsometric measurements. It is a typical 2-mW laser whose linearly polarized output beam is converted to circular polarized light and is expanded and collimated to just over 10 mm. The uncertainty in the wavelength, 632.82 nm, as shown in Table I is $\pm$0.01 nm and is given as a systematic error.

Goniometer Calibration Uncertainty

The two goniometers that control the azimuth of the polarizer and the angle of incidence of the sample were calibrated to correct for the difference between their true angular positions and their encoder readout dial positions [12]. Each goniometer is computer-controlled by a stepping motor and encoder. A calibration curve for each goniometer was determined and stored in the computer so that all angular dial readings are corrected to within a systematic component of uncertainty of $\pm$0.001°. All goniometer angular positions are reached in the same direction of rotation to prevent an uncertainty due to the small amount of backlash in the goniometer motor drive system.

Angle-of-Incidence Uncertainty, $\delta\phi$

The angle of incidence is determined by interferometrically aligning the surface of the sample normal to the incident laser beam and then using a calibrated goniometer to rotate the sample to a given angle of incidence. This alignment procedure is as follows. First, the surface of the sample is aligned very close to normal incidence by rotating its goniometer and recording the dial reading. Then fine adjustments in the two-axis wafer stage are made in the horizontal angular position, affecting the angle of incidence, and also in the vertical tilt, affecting the polarizer and analyzer azimuths, to null or minimize the number of fringes viewed by means of a beam splitter permanently mounted between the laser and polarizer element and a TV monitor. These fringes are caused by the interference between the reflected laser beam from the wafer's surface and the reflected return beam from the laser's exit window surface. This alignment at normal incidence is accurate and reproducible to within $\pm 0.002°$ in the plane of incidence and also $\pm 0.002°$ in the tilt of the plane of incidence as shown in Table I. The tilt uncertainty causes an uncertainty in azimuth alignment of both polarizer and analyzer. The angle-of-incidence uncertainty results in a systematic error for a particular single set of measurements on a wafer, but for repeated mountings of a given sample or for a set of samples, it is a random error. The random uncertainty associated with the beam direction stability of the laser was found to be neglible for this ellipsometer.

There are three other components of systematic uncertainties in the angle of incidence. As stated, the calibration of the goniometer produces a systematic uncertainty of $\pm 0.001°$. In addition, the initial beam deviation through the polarizer in transmission, $0.010°$, was corrected to be less than $\pm 0.001°$ with the addition of an optical wedge plate attached to the polarizer on the entrance beam side. The uncertainty associated with beam divergence, because of collimation, is negligible.

Analyzer Encoder Pulse Uncertainty

The analyzer prism is housed in a hollow shaft optical encoder. This incremental encoder gives the location of the analyzer azimuth that is rotating at approximately 50 rpm. It has a once-per-revolution zero reference or trigger pulse in addition to 4096 uniformly spaced incremental pulses that are accurate to $\pm 0.001°$. A divide-by-eight circuit is used to allow 512 pulses per revolution to trigger the capture of the intensity signal as a function of the analyzer's position.

Azimuth Alignment Uncertainties, δP_c and δA_c

The calcite polarizer and analyzer prism elements are of the Glan-Thompson type and have an extinction coefficient of approximately 10^{-6}. These polarizing prisms must be calibrated to determine the correction necessary to place their transmissive axes into the same zero azimuth as defined by the plane of incidence. This procedure is described in detail in references 10 and 11 and is outlined here. The true polarizer azimuth position, P, and analyzer azimuth position, A, are obtained from their respective goniometer or encoder azimuth positions by adding to that reading the correction or offset component,

P_c or A_c. The offset in the analyzer results in a phase shift of the intensity signal at th detector. Thus the Fourier coefficients, α and β in eq. (6), are transformed from the Fourie coefficients computed from the measured intensity signal. Calibration measurements ar taken to determine these offset angles for the polarizer transmissive axis azimuth and it goniometer's zero dial reading and the analyzer transmissive axis azimuth and its zero point optical encoder signal. These measurements were performed within a few degree of the principal angle of incidence of each wafer to be characterized. Performing th calibration measurements at this angle of incidence minimizes the effect of residual polarize ellipticity [11]. Each measurement procedure involves sweeping the polarizer $\pm 2.5°$ abou its estimated 0° azimuth position in steps of 0.5°, and at each position obtaining value for the measured Fourier coefficients. A calibration is made by fitting the values of eac expression, $(\bar{\alpha}^2 + \bar{\beta}^2)$ and $\tan^{-1}(\bar{\alpha}/\bar{\beta})$, versus the polarizer position where $\bar{\alpha}$ and $\bar{\beta}$ ar the averaged coefficients obtained from discrete Fourier transforms on the intensity signa (eq. (A1.12)). Repetitions of the calibration measurement are then analyzed to determin the mean values of P_c and A_c, and the resulting standard deviations are used to evaluat the offset uncertainties, δP_c and δA_c. Typical values for both δA_c and δP_c are ± 0.002 These are listed in Table I as systematic uncertainties for a single measurement but ca become random uncertainties for repeated measurements.

Polarizer Ellipticity

The polarizer ellipticity was estimated to be approximately 0.010° from many measur ments made in two zones, polarizer azimuth settings of $+P$ and $-P$ [13]. This ellipticit is typical for a good polarizer (ref. 9, p. 389). After zone averaging, the effects of th polarizer ellipticity become negligible.

Detector Nonlinearity and Other Intensity Signal Effects

The detector used with the helium-neon laser for the intensity measurements is a sil con photodiode. The nonlinear response of this detector and its amplifying circuit [14 although very small, was minimized by working near the principal angle of inciden and having the polarizer azimuth close to ψ, in which case the alternating compone of detected-light intensity is near zero. Careful beam alignment with the axis of rotatic of the analyzer prism ensured a signal that contained only the dc and second harmon signal. The background signal level, obtained when the laser light intensity is extinguishe was found to be negligible compared to the resolution of the detection system.

Table I

Instrumental Components of Uncertainty

Quantity	Systematic	Random
Wavelength uncertainty, $\delta\lambda$	$\pm$0.01 nm	
Angle-of-incidence uncertainty, $\delta\phi$		
Sources of uncertainty:		
ϕ goniometer calibration	$\pm$0.001°	
Sample alignment (in plane of incidence)		$\pm$0.002°
Polarizer beam deviation	$\pm$0.001°	
Polarizer azimuth uncertainty, δP		
Sources of uncertainty:		
P goniometer calibration	$\pm$0.001°	
Sample alignment (tilt of plane of incidence)		$\pm$0.002°
Transmissive axis azimuth alignment, δP_c	$\pm$0.002°	
Analyzer azimuth uncertainty, δA		
Sources of uncertainty:		
Sample alignment (tilt of plane of incidence)		$\pm$0.002°
A encoder pulse uncertainty	$\pm$0.001°	
Transmissive axis azimuth alignment, δA_c	$\pm$0.002°	
Polarizer ellipticity (after zone averaging)	negligible	
Detector nonlinearity (at principal angle of incidence)	negligible	

V. Analysis of the Fourier Coefficients

The zone-averaged Fourier coefficients, α' and β', are defined by eqs. (A1.20) and (A1.21) in Appendix 1. Both the short-term and long-term precision were evaluated by computing the standard deviations of the zone-averaged Fourier coefficients. The short-term repeatability is equivalent to the resolution of the instrument, and the long-term repeatability is the major contribution to the uncertainty in the measurement.

Short-term precision and resolution

The precision or resolution of measurement for the rotating analyzer ellipsometric method is obtained from short-term repeated measurements taken on an SRM sample. Standard

deviations of zone-averaged values, α' and β', give the limiting resolution of the inst ment. The random fluctuations of the light source and the detector response, which occ during the time it takes to make a single determination, and the resolution of the 12-l analog-to-digital converter affect these standard deviations. The time duration for ea zone measurement consisting of 32 revolutions of the analyzer is approximately 0.5 s, which time the 512 points per revolution times 32 revolutions analog-to-digital intensi conversions take place. Ten consecutive zone-averaged measurements of α' and β' c take approximately 20 minutes because of the time it takes the stepper motor to move t polarizer from zone one to zone two. The standard deviations of these measurements, δ and $\delta\beta'$, made on an SRM sample are listed in Table II.

Long-term precision and uncertainty

In the long-term measurements, each sample was mounted, cleaned, and measured both the right and left sides. This procedure was repeated an average of 5 times for ea sample. These long-term measurements were performed on 6 samples, 2 each from tl three thickness groups, 50, 100, and 200 nm of silicon dioxide. A total of 62 measuremen were made over a period of 1 month. The measurements were made at the same ang of incidence and polarizer settings for samples of each thickness. The variations in and β' may include fluctuations caused by slight variation in cleaning the surface, samp remounting angle-of-incidence fluctuations, measurement area positioning uncertaintie and possible instrumental drift due to warm-up time. The long-term standard deviation $s_{\alpha'}$ and $s_{\beta'}$, of α' and β' are used to determine the uncertainties in Δ and ψ for SR certification.

Table II

Short- and Long-Term Precision in the Fourier Coefficients

	Radians	Degrees	Radians	Degrees	DF*
	$\delta\alpha'$		$\delta\beta'$		
Short-term precision	0.0001	0.006°	0.0001	0.006°	9
	$s_{\alpha'}$		$s_{\beta'}$		
Long-term precision	0.0012	0.069°	0.0006	0.034°	50

*degrees of freedom

VI. Uncertainties in the Ellipsometric Parameters

The uncertainties in the zone-averaged quantities Δ' and ψ' depend upon various contributions, such as uncertainties in the Fourier coefficients, $\delta\alpha'$ and $\delta\beta'$; in the polarizer azimuth, δP; in the angle of incidence, $\delta\phi$; and in the wavelength, $\delta\lambda$. The following expressions for the uncertainty in Δ' and ψ' due to $\delta\alpha'$, $\delta\beta'$, and the systematic uncertainty in δP are shown from eqs. (A1.24) and (A1.25) in Appendix 1 to be

$$\delta\psi' \leq \left|\frac{1}{1-\alpha'\cos 2P}\right| \left[\left|\delta P\ \sqrt{1-\alpha'^{\,2}}\right| + \left|\delta\alpha'\ \frac{\sin 2P}{2\sqrt{1-\alpha'^{\,2}}}\right|\right] \tag{11}$$

and

$$\delta\Delta' \leq \frac{1}{\sqrt{1-\alpha'^{\,2}-\beta'^{\,2}}} \left[\left|\delta\alpha'\ \frac{\alpha'\beta'}{1-\alpha'^{\,2}}\right| + |\delta\beta'|\right]. \tag{12}$$

When measurements are taken close to the principal angle of incidence [15], ϕ_p, where $\Delta = 90°$, and $P = \psi$, the light intensity as a function of the analyzer angle has minimal fluctuation and α' and β' are both near zero. At these settings, any small nonlinearity of the detector does not contribute an error to the α' and β' terms. Also, because $\alpha' \simeq 0$ and $\beta' \simeq 0$, and because $|\sin 2P| \leq 1$, eqs. (11) and (12) reduce in first order to the following:

$$\delta\psi' \leq \left|\frac{\delta\alpha'}{2}\right| + |\delta P| \tag{13}$$

and

$$\delta\Delta' \leq |\delta\beta'|\,. \tag{14}$$

The measurements are taken near the principal angle because the values of $\delta\psi'$ and $\delta\Delta'$ are at a minimum.

All systematic and random contributions to the total uncertainties in Δ' and ψ' are calculated from eqs. (A1.28) and (A1.29) and are listed in Table III. The effect of the systematic component of uncertainty in the wavelength is negligible. The systematic component of uncertainty in the angle of incidence is taken to be $\pm 0.002°$, arising from the ϕ goniometer calibration and polarizer beam deviation contribution of uncertainties as given in Table I. Random sample alignment variations affect the long-term repeated measurements and therefore are included only in the standard deviations of α' and β'. The uncertainties in Δ' and ψ' arising from the angle of incidence uncertainty are listed as upper-limit values for all three SRM thickness categories.

The polarizer azimuth systematic component of uncertainty, $\pm 0.003°$, arises from both the goniometer calibration and transmissive axis alignment contribution of uncertainties

as shown in Table I. Equations (13) and (14) give the contribution to the uncertainties $\delta\Delta$ and $\delta\psi'$ as given in Table III. The long-term standard deviations, $s_{\alpha'}$ and $s_{\beta'}$, from Table II are used with eqs. (13) and (14) to obtain the contribution of the Fourier coefficients to the uncertainties, listed in Table III.

Table III

Systematic and Random Contributions to the Uncertainties in Δ' and ψ'

	Systematic	Random	$\delta\Delta'$	$\delta\psi'$
Wavelength, $\delta\lambda$	$\pm$0.01 nm	——	$\pm$0.000°	$\pm$0.000°
Angle of incidence, $\delta\phi$	$\pm$0.002°	——	$\pm$0.008°	$\pm$0.001°
Polarizer azimuth, δP	$\pm$0.003°		——	$\pm$0.003°
$s_{\alpha'}$ (0.0012 radians)		0.069°	——	$\pm$0.035°
$s_{\beta'}$ (0.0006 radians)		0.034°	$\pm$0.034°	——
			$\delta\Delta'_T$ *	$\delta\psi'_T$ *
Total			$\pm$0.042°	$\pm$0.039°

*The total uncertainties, $\delta\Delta'_T$ and $\delta\psi'_T$, for each wafer are reported on the certificate that accompanies each SRM as one-standard-deviation limits to random error plus systematic error; the one-standard-deviation limits to random error correspond to a confidence coefficient of 0.68. The prime superscripts have been omitted on the certificate.

VII. Description of the Least-Squares Analysis

In order to go from ellipsometer parameters Δ and ψ to material parameters of thickness and index, the data have to be processed through a model. The least-squares problem of comparing experimental measurement with a model is formulated in Appendix 2. The following expression, eqs. (A2.3) and (A2.4),

$$|\mathbf{g}| = \sqrt{\frac{1}{2M}\sum_{i=1}^{M}\left[(\Delta_i' - \Delta_i'')^2 + (\psi_i' - \psi_i'')^2\right]}, \tag{15}$$

involving the deviations between the measured values, ψ' and Δ', and the modeled values, ψ'' and Δ'', is minimized. The sum is over M total measurements including different samples and angles of incidence. This least-squares analysis was applied to the two-layer and one-layer models.

VIII. Parameters of the Two-Layer Model

The following least-squares-fitting procedure was used in determining the parameters for the SRM's. In analyzing the two-layer model, all the data obtained on all the samples for the three silicon dioxide thicknesses, 50, 100, and 200 nm, were analyzed collectively. As stated in section II, all the wafers were obtained from the same silicon ingot, and all the silicon dioxide films were grown under the same conditions except for the length of time for dry silicon dioxide growth. The layer parameters that are varied in the least-squares analysis are determined when $|\mathbf{g}|$ is at a minimum. At this minimum, the deviations between the measured and modeled Δ's and ψ's should be on the order of the measurement uncertainties in Δ' and ψ'.

A depiction of the two-layer model is shown in Figure 2. The model involves a thin interlayer between the silicon substrate and silicon dioxide layer. Two parameters, common to all samples, that were not estimated from the measurement data were the imaginary part of the silicon substrate refractive index, $k_s = 0.018$ [8], and the interlayer refractive index, $n_i = 2.8$ [5-7]. The model parameters that were estimated by least squares include the silicon dioxide layer thickness, t_f, for each sample and the following parameters, common among all samples: the silicon dioxide layer refractive index, n_f; the interlayer film thickness, t_i; and the real part of the silicon substrate refractive index, n_s. The imaginary part of the silicon dioxide layer refractive index at 632.8 nm is zero, and it was found that setting the imaginary part of the interlayer refractive index to zero had negligible effect on the least-squares fit.

From a total of 239 ellipsometric measurements on 52 samples, including left and right side and long-term repeated measurements, the best estimates from the least-squares analysis

Table IV

Parameters and Uncertainties for the Two-Layer Model†

Values from the Least-Squares Analysis

	Sample Serial No. 390-03	384-48	389-10		All Samples	
	t_f	t_f	t_f	t_i	n_f	n_s
$\lvert\mathbf{g}\rvert$ [a,b,c] $= 0.068°$	53.9	97.9	202.3	1.0	1.461	3.875

Contributions to Total Uncertainties from the Sensitivity Analysis

	δt_f	δt_f	δt_f	δt_i	δn_f	δn_s
s_g [d] $= 0.078°$	±0.11	±0.13	±0.18	±0.03	±0.0003	±0.0011
s_ϕ [e] $= 0.002°$	±0.02	±0.01	±0.01	±0.01	±0.0000	±0.0001
δk_s [f] $= \pm 0.005$	±0.01	±0.01	±0.01	±0.09	±0.0000	±0.0001
δn_i [f] $= \pm 0.4$	±0.06	±0.06	±0.06	±0.21	±0.0000	±0.0010
Total [g]	±0.18	±0.20	±0.25	±0.33	±0.0003	±0.0022

Final Values and Their Uncertainties*

	$t_f + t_i$	$t_f + t_i$	$t_f + t_i$	t_i	n_f	n_s
	54.9	98.9	203.3	1.0	1.461	3.875
	$\delta(t_f + t_i)$	$\delta(t_f + t_i)$	$\delta(t_f + t_i)$	δt_i	δn_f	δn_s
	±0.5	±0.5	±0.6	±0.3	±0.001	±0.003

†Thicknesses in nanometers

[a] See eq. (15)

[b] $k_s = 0.018$, see ref. 8

[c] $n_i = 2.8$, see refs. 5, 6, and 7

[d] Random component of uncertainty, see eq. (A3.8)

[e] Random component of uncertainty (Systematic component of ±0.002° gives negligible effect)

[f] Systematic components of uncertainty

[g] See eq. (A3.7) for the calculation of the total uncertainties

*The total uncertainties for each wafer are reported on the certificate that accompanies each SRM. The uncertainties are computed as one-standard-deviation limits to random error plus systematic error; the one-standard-deviation limits to random error correspond to a confidence coefficient of 0.68.

for the model parameters are shown in the first row of numbers in Table IV. Three representative samples (Sample Nos. 390-03, 384-48, and 389-10) are shown. The value for the least-squares parameter, $|\mathbf{g}|$, is 0.068°. The following common parameter values are found: interlayer thickness t_i, 1 nm; the refractive index of the silicon dioxide film n_f, 1.461; and the value of the silicon substrate refractive index n_s, 3.875.

IX. Sensitivity Analysis and Uncertainties in the Model Parameters

In Appendix 3, a sensitivity analysis of the model parameters is discussed. The manner in which one may associate an uncertainty with the model parameters is developed leading to eq. (A3.7). Using the sensitivity analysis, the value of $s_g = 0.078°$, the standard deviation in the angle of incidence, $s_\phi = 0.002°$ (random part of uncertainty in Table I), the systematic part of the angle of incidence uncertainty, $\delta\phi_{sys} = 0.002°$, an uncertainty of $\delta k_s = \pm 0.005$ [8,16] for the value of $k_s = 0.018$, and the uncertainty in the interlayer refractive index of $\delta n_i = \pm 0.4$ [5-7] for the value of $n_i = 2.8$, the relative contributions to the total uncertainties in the model parameters can be found.

The second row of Table IV, labeled s_g, gives random components of uncertainties in the estimated model parameters due to the fit of the measured data. The next row labeled s_ϕ gives the contribution of uncertainty due to the random component of angle of incidence uncertainty (systematic component of $\pm 0.002°$ gives negligible effect). Rows labeled δk_s and δn_i give the respective contribution to the systematic components of uncertainties.

The value of this sensitivity analysis is that the contributions to the uncertainties can be pinpointed. The two largest sources of uncertainty in the thickness of the total oxide arise from the value of s_g obtained from the measurement fit and from the large uncertainty in the thickness of the interlayer due to δn_i. The large uncertainty in the interlayer thickness arises from the correlation of the refractive index and the thickness for this very thin film.

X. Parameters of the One-Layer Model

Two different one-layer models have been analyzed. The first model assumes a common value of refractive index, independent of layer thickness, to all SRM samples. The second model allows a different common value of refractive index for each layer thickness group of SRM's. The experimental fit to the first model is very poor (see sec. XI). The second model, which gives a layer refractive index that is different for each of the three thickness categories of SRM's, 50, 100, and 200 nm, is not physically realistic, but is commonly used when processing single-sample data and is therefore given as supplementary information on the certificate.

The three thickness categories of SRM wafers, 50, 100, and 200 nm, were analyzed separately by the least-squares procedure using this second single-layer model. All SRM's of the same thickness group were allowed to have a best-fit common refractive index, n_f, of the film, and a best-fit common substrate refractive index, n_s, and a fixed common

value for k_s. An individual thickness was calculated for each wafer. The value of n_s was found to be the same as that of the two-layer model, $n_s = 3.875$, and the corresponding film refractive indices, n_f for the 50-, 100-, and 200-nm wafers, were 1.468, 1.465, and 1.458, respectively. For the samples in Table IV, the one-layer model thicknesses for serial numbers 390-03, 384-48, and 389-10 are 54.4, 98.1, and 204.0 nm, respectively. These film thicknesses should be compared with the two-layer calculation that includes the thickness of the interlayer as given under "Final Values and Their Uncertainties" in Table IV. The two-layer model and the one-layer model for the 50-, 100-, and 200-nm samples disagree by the amounts 0.5, 0.8, and 0.7 nm, respectively.

XI. Goodness-of-Fit Test

Three distinct models were considered and discussed earlier in the text, i.e., two one-layer models and a two-layer model. The one-layer model considered in this section assumes a common value of layer refractive index, independent of thickness. The two-layer model has an interlayer between the top silicon dioxide film and silicon substrate. The model parameters of this interlayer include its refractive index (n_i) and thickness (t_i). Hence, the two-layer model requires two parameters more than the one-layer model.

It is important to test the fit of the experimentally measured ellipsometric parameters Δ' and ψ' to those predicted by the nonlinear model used for estimating individual specimen thicknesses and indices of refraction. This is done independently for each model using a goodness-of-fit procedure that is outlined in Appendix 4. An F statistic for testing for lack of fit is given by eq. (A4.4),

$$F = \frac{[SS_{total\ error} - SS_{pure\ error}] / [df_{total\ error} - df_{pure\ error}]}{[SS_{pure\ error}] / [df_{pure\ error}]}, \tag{16}$$

where the SS stands for the sum of squares of the errors (see eqs. (A4.1) and (A4.3)) and df are the degrees of freedom as defined in Appendix 4. The F statistic is compared with $F_\alpha(\nu_1, \nu_2)$ which represents the upper α percent point of the F distribution with ν_1 and ν_2 degrees of freedom. The F test is not exact because the underlying model is nonlinear; however, a value of

$$F \leq F_\alpha(\nu_1, \nu_2), \tag{17}$$

indicates that there is no significant lack of fit to the collective data for the model being considered.

The pure error term is constructed from repetitions on six specimens that were remeasured several times at the same wavelength and the same angle of incidence over the course of the calibration of the batch of SRM's. The degrees of freedom associated with the pure

error term is $\nu_2 = 92$. The total error term is constructed from the deviations from the fit with 377 degrees of freedom for the two-layer model; the sum of squares for lack of fit has degrees of freedom equal to the degrees of freedom for total error minus the degrees of freedom for pure error, or $\nu_1 = 285$.

The value of F from eq. (16) is 3.8 for the two-layer model. For a significance level of $\alpha = 0.01$, the corresponding critical value for $F_{.01}(285, 92)$ is 1.5. The F statistic, which is very sensitive to lack of fit or large outliers, exceeds the critical value but not by enough to indicate an egregious lack of fit. The goodness-of-fit test indicates that the two-layer model adequately represents the wafer's surface. The F statistic is 21.4 for the corresponding one-layer model or five times greater than for the two-layer model, indicating a much greater degree of lack of fit to the model.

XII. Computer Program for Determining the Thickness of the SRM Silicon Dioxide Layer

Accompanying this SRM-2530 is a floppy disk formatted on an IBM PC/XT that contains a computer program. This program is a combination of McCrackin's method [17] followed by a least-squares method for calculating the thickness of the SRM silicon dioxide layer. In Appendix 4, a description is included of how to use this program to calculate the thickness for both the one- and two-layer models.

Acknowledgments

The authors thank James R. Ehrstein for initial work on concept of this SRM, for numerous discussions, and for continued interest; Mary Lou Miller for assistance in the fabrication of the SRM; and members of the CALCOM subcommittee, in particular, its chairman, Robert D. Larrabee.

References

1. Candela, G.A., and Chandler-Horowitz, D., An ellipsometry system for high accuracy metrology of thin films, SPIE **480**, Integrated Circuit Metrology II, 2-8 (1984).

2. Candela, G.A., Chandler-Horowitz, D. Novotny, D.B., Vorburger, T.V., and Giauque, C.H.W., Film thickness and refractive index Standard Reference Material calibrated by ellipsometry and profilometry, SPIE **661**, Optical Testing and Metrology, 402-407 (1986).

3. Ehrstein, J.R., Some Considerations Regarding Film Thickness Standards for the Semiconductor Industry, NBSIR 80-2158 (November 1980).

4. Chandler-Horowitz, D., Semiconductor Measurement Technology: Analytic analysis of ellipsometric errors, NBS Special Publication 400-78 (May 1986).

5. Taft, E., and Cordes, L., Optical evidence for a silicon-silicon oxide interlayer, Journa of the Electrochemical Society: Solid-State Science and Technology **126**, No. 1, 131 134 (January 1979).

6. Theeten, A.B., and Aspnes, D.E., The determination of interface layers by spectro scopic ellipsometry, Thin Solid Films **60**, 183-192 (1979).

7. Pedinoff, M.E., and Stafsudd, O.M., Multiple angle ellipsometric analysis of surfac layer contaminants, Applied Optics **21**, No. 3, 518-521 (1 February 1982).

8. Handbook of Constants of Solids, E.D. Palik, Ed. (Academic Press, Orlando, 1985)

9. Azzam, R.M.A., and Bashara, N.M., Ellipsometry and Polarized Light (North Ho land, Amsterdam, 1987).

10. Hauge, P.S., and Dill, F.H., Design and operation of ETA, an automated ellipsomete IBM Journal of Research and Development **17**, No. 6, 472-489 (November 1973).

11. Aspnes, D.E., and Studna, A.A., High precision scanning ellipsometer, Applied Opti **14**, No. 1, 220-228 (1975).

12. Reeve, C.P., The Calibration of Indexing Tables by Subdivision, NBSIR 75-750 (Ju 1975).

13. McCrackin, F.L., Passaglia, E., Stromberg, R.R., and Steinberg, H.L., Measureme of the thickness and refractive index of very thin films and the optical properties surfaces by ellipsometry, NBS J. Res. – A. Physics and Chemistry **67A**, 363-3 (July-August 1963).

14. Aspnes, D.E., Spectroscopic ellipsometry of solids, Chapter 15, Optical Properties Solids – New Developments, B.O. Seraphin, Ed. (North-Holland Publishing Compar Amsterdam, 1976), pp. 799-846.

15. Chandler-Horowitz, D., and Candela, G.A., Principal angle spectroscopic ellipsomet utilizing a rotating analyzer, Applied Optics **21**, 2972-2977 (15 August 1982).

16. Aspnes, D.E., Studna, A.A., and Kinsbron, E., Dielectric properties of heavily dop crystalline and amorphous silicon from 1.5 to 6.0 eV, Physical Review B **29**, 768-7 (January 1984).

17. McCrackin, F.L., A FORTRAN program for analysis of ellipsometer measuremen NBS Technical Note 479 (1969).

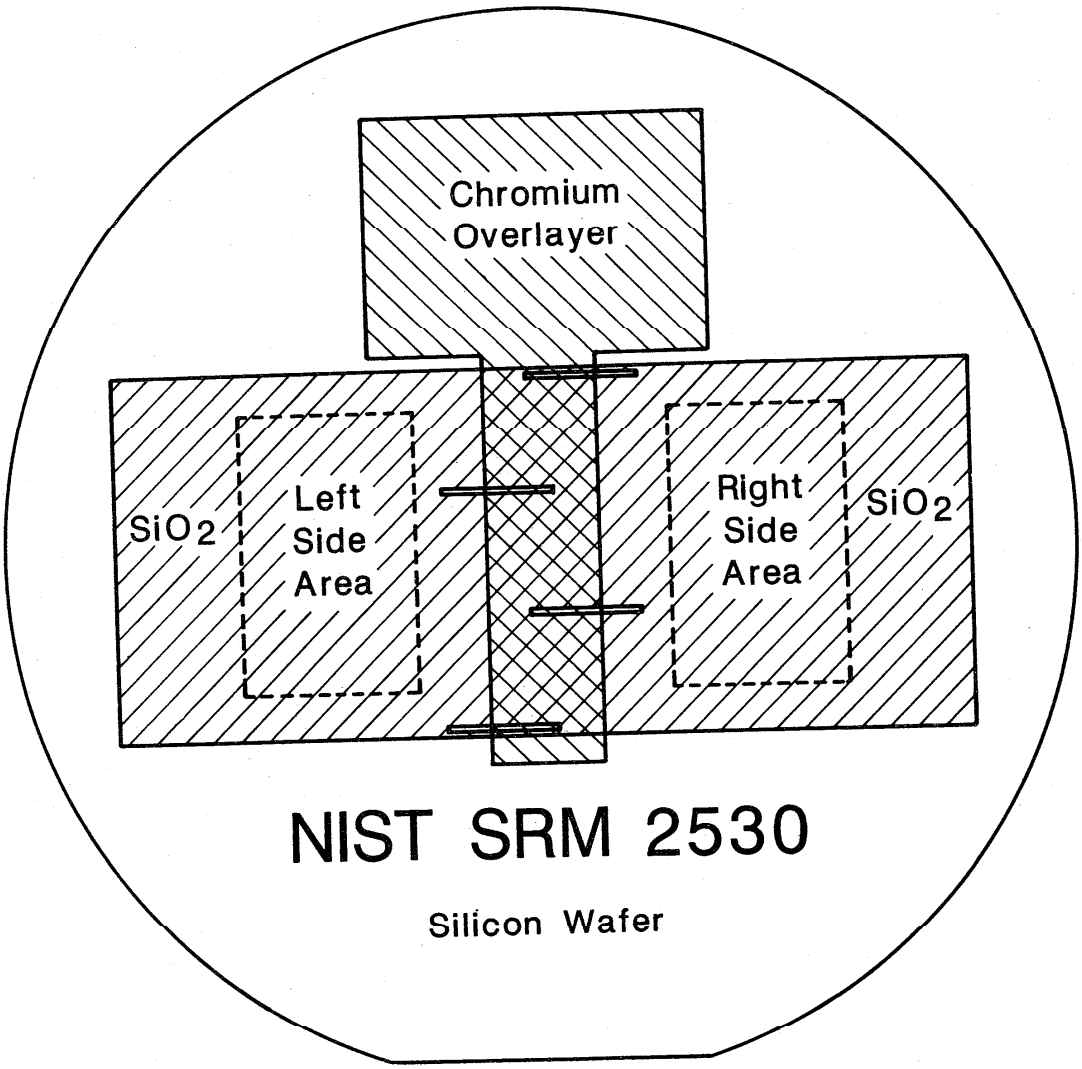

Figure 1. Schematic of SRM-2530. The ellipsometric measurements were performed within the outlined right and left areas.

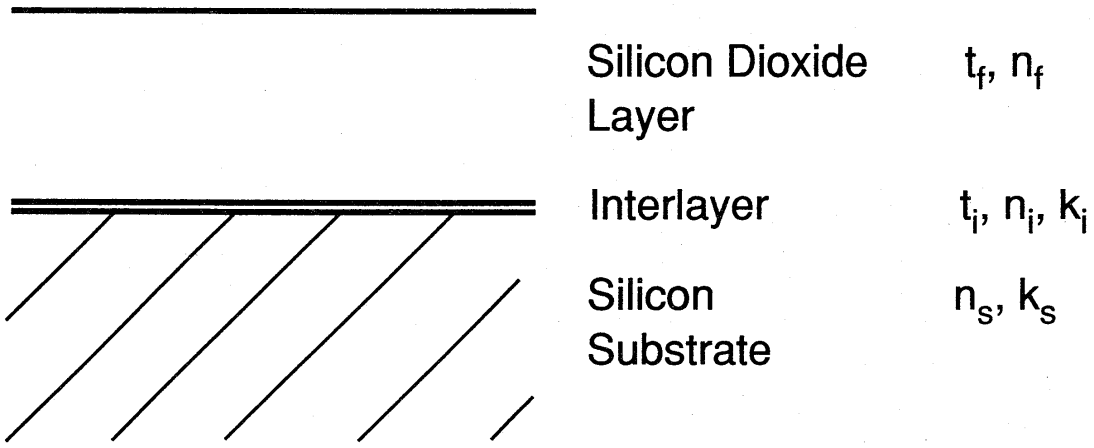

Figure 2. Schematic of two-layer model. Cross-section schematic of silicon dioxide on silicon designating seven of the parameters for the two-layer model. The one-layer mod assumes that no interlayer is present, $t_i = 0$.

Appendix 1

Ellipsometer Precision and Uncertainty

All ellipsometric measurements on the Standard Reference Materials were obtained by an ellipsometer using the rotating analyzer configuration. Here, a simple discussion is presented regarding the precision and uncertainty of the instrumentation in order to obtain the uncertainty in the two ellipsometric parameters, Δ and ψ. An assessment is made of the various random and systematic uncertainties which contribute to the total uncertainty of Δ and ψ. In this appendix, no assessment is made regarding the effects due to sample preparation, mounting, or alignment, e.g., relocating the illuminated spot on the sample during remounting or those effects due to cleaning the surface of the sample. These issues are discussed in section IV.

For the case of the rotating analyzer ellipsometer, the intensity flux of light, I(t), at the detector is a known function of time and is given by

$$I(t) = I_0\big(1 + \alpha \cos 2A(t) + \beta \sin 2A(t)\big), \qquad (A1.1)$$

where $A(t)$ refers to the azimuth angle of the transmissive axis of the analyzer, is measured with respect to the plane of incidence, is a function of time, t, and is given by

$$A(t) = 2\pi f t + A_c. \qquad (A1.2)$$

Here, I_0 is the average intensity, α and β are the normalized Fourier coefficients, f is the mechanical rotation frequency, and A_c is a constant phase factor. The two Fourier coefficients represent contributions of the second harmonic to the measured intensity. Also, the measured intensity is known to be a function of the polarizer azimuth, P, so that the phase and amplitude information of the reflected light, ψ and Δ, may be expressed by [A1.1]

$$\psi = \tan^{-1}\left[\sqrt{\frac{1+\alpha}{1-\alpha}}\,\left|\tan P\right|\right], \qquad 0 \le \psi \le 90^\circ \qquad (A1.3)$$

and

$$\Delta = \pm\cos^{-1}\left[\sqrt{\frac{\beta^2}{1-\alpha^2}}\,\right], \qquad -180^\circ < \Delta \le 180^\circ\,. \qquad (A1.4)$$

In order to determine α and β from experiment, the intensity flux is sampled at 512 discrete equally spaced points of azimuth angle per mechanical revolution of the analyzer. The analyzer's relative azimuth angle is obtained from encoder pulses triggered by a zero reference signal from its hollow shaft optical encoder. Data are collected for 32 revolutions of the analyzer.

Within each mechanical revolution of the analyzer, the measured intensities are assumed to be of the form

$$I_j = a_0 + a_2 \cos 2A_j + b_2 \sin 2A_j + e_{jk} \tag{A1.5}$$

$$= a_0\left(1 + \alpha \cos 2A_j + \beta \sin 2A_j\right) + e_{jk}, \tag{A1.6}$$

where

$$A_j = 2\pi\frac{(j-1)}{J}, \qquad j = 1, 2, \ldots, J, \tag{A1.7}$$

where J is equal to 512 and K is equal to 32, and where j indexes the discrete positions of azimuth angle of the analyzer, k indexes the revolutions of the analyzer, and e_{jk} is due to small fluctuations of random noise.

A method of least squares is then used to provide a best estimate of a_0, a_2, and b_2. Letting I_{jk} denote the measured intensity at the j^{th} value of azimuth angle and k^{th} revolution of the analyzer, a discrete Fourier transform is performed where

$$a_{0k} = \frac{1}{J}\sum_{j=1}^{J} I_{jk}, \qquad \bar{a}_0 = \frac{1}{K}\sum_{k=1}^{K} a_{0k}, \tag{A1.8}$$

$$a_{2k} = \frac{2}{J}\sum_{j=1}^{J} I_{jk} \cos 2A_j, \qquad \bar{a}_2 = \frac{1}{K}\sum_{k=1}^{K} a_{2k}, \tag{A1.9}$$

$$b_{2k} = \frac{2}{J}\sum_{j=1}^{J} I_{jk} \sin 2A_j, \qquad \bar{b}_2 = \frac{1}{K}\sum_{k=1}^{K} b_{2k}, \tag{A1.10}$$

and

$$\alpha_k = \frac{a_{2k}}{a_{0k}}, \qquad \beta_k = \frac{b_{2k}}{a_{0k}}, \tag{A1.11}$$

$$\bar{\alpha} = \frac{\bar{a}_2}{\bar{a}_0}, \qquad \bar{\beta} = \frac{\bar{b}_2}{\bar{a}_0}. \tag{A1.12}$$

The standard deviations of α and β are estimated by

$$s_\alpha = \sqrt{\frac{1}{K-1}\sum_{k=1}^{K}(\alpha_k - \bar{\alpha})^2} \qquad (A1.13)$$

and

$$s_\beta = \sqrt{\frac{1}{K-1}\sum_{k=1}^{K}(\beta_k - \bar{\beta})^2}. \qquad (A1.14)$$

The statistical uncertainty associated with determining the normalized Fourier coefficients, $\bar{\alpha}$ and $\bar{\beta}$, is assumed or defined to be

$$\delta\bar{\alpha} = s_\alpha \qquad \text{and} \qquad \delta\bar{\beta} = s_\beta. \qquad (A1.15)$$

There is an inherent angular or phase offset between the intensity detected at the first encoded pulse and that associated with the true zero azimuth of the analyzer. This is due to two distinct conditions, one being a mechanical offset in the mounting of the analyzer in the optical encoder, and the other being a phase lag in the signal processing circuits. Together, their net effect is that of inducing a simple coordinate rotation onto the analyzer though an effective angle, A_c, and an amplitude reduction, which for this ellipsometer, was negligible. By following a simple calibration procedure [A1.2], this angular offset (A_c) is determined. Then, the calibrated normalized Fourier coefficients become

$$\alpha_c = \bar{\alpha}\cos 2A_c + \bar{\beta}\sin 2A_c, \qquad (A1.16)$$

$$\beta_c = \bar{\alpha}\sin 2A_c + \bar{\beta}\cos 2A_c, \qquad (A1.17)$$

and their corresponding uncertainties

$$\delta\alpha_c \le \left|\delta\bar{\alpha}\cos 2A_c\right| + \left|\delta\bar{\beta}\sin 2A_c\right| + 2\left|\delta A_c(\bar{\alpha}\sin 2A_c - \bar{\beta}\cos 2A_c)\right|, \qquad (A1.18)$$

$$\delta\beta_c \le \left|\delta\bar{\alpha}\sin 2A_c\right| + \left|\delta\bar{\beta}\cos 2A_c\right| + 2\left|\delta A_c(\bar{\alpha}\cos 2A_c - \bar{\beta}\sin 2A_c)\right|. \qquad (A1.19)$$

The last term in each of the above two equations depends on the uncertainty in the analyzer offset value (δA_c), but is negligible when compared to the first and second terms when $\bar{\alpha}$ and $\bar{\beta}$ are small and of the order of $\delta\bar{\alpha}$ or $\delta\bar{\beta}$ at the principal angle of incidence.

Furthermore, these values (α_c, β_c) are determined at a specific position setting (P) of the polarizer, and hence depend upon P. Also, it is known that most polarizers are imperfect and contain some inherent ellipticity. So, to correct for this systematic error as well as for azimuth calibration uncertainties in the polarizer, one performs a procedure called zone averaging. This is accomplished by determining the Fourier coefficients (α_c, β_c) at the positive polarizer setting $(+P)$, which may be denoted by (α^+, β^+), as well as at the negative polarizer setting $(-P)$, denoted by (α^-, β^-). The zone-averaged values are defined by

$$\alpha' = \frac{(\alpha^+ + \alpha^-)}{2} \tag{A1.20}$$

and

$$\beta' = \frac{(\beta^+ - \beta^-)}{2}. \tag{A1.21}$$

The negative sign present in eq. (A1.21) is due to the fact that β is an odd function of the polarizer azimuth P, as may be seen from eq. (8). The corresponding uncertainties are

$$\delta\alpha' \leq \frac{|\delta\alpha^+| + |\delta\alpha^-|}{2} \tag{A1.22}$$

and

$$\delta\beta' \leq \frac{|\delta\beta^+| + |\delta\beta^-|}{2}. \tag{A1.23}$$

Knowing α', β', P, and eqs. (A1.3) and (A1.4), one may then calculate zone-averaged estimates, Δ' and ψ', of Δ and ψ. Accordingly, it also follows that the uncertainties may be estimated by

$$\delta\psi' \leq \left| \frac{1}{1 - \alpha' \cos 2P} \right| \left[\left| \delta P \sqrt{1 - \alpha'^2} \right| + \left| \delta\alpha' \frac{\sin 2P}{2\sqrt{1 - \alpha'^2}} \right| \right] \tag{A1.24}$$

and

$$\delta\Delta' \leq \frac{1}{\sqrt{1 - \alpha'^2 - \beta'^2}} \left[\left| \delta\alpha' \frac{\alpha'\beta'}{1 - \alpha'^2} \right| + |\delta\beta'| \right]. \tag{A1.25}$$

For ellipsometric data taken at the principal angle of incidence, $\Delta' = \pm 90°$, and with the polarizer azimuth, $P = \psi'$, α' and β' are small and eqs. (A1.24) and (A1.25) reduce to

$$\delta\psi' \leq \frac{\delta\alpha'}{2} |\sin 2P| + \delta P \leq \left| \frac{\delta\alpha'}{2} \right| + |\delta P| \tag{A1.26}$$

and

$$\delta\Delta' \leq |\delta\beta'|\,. \qquad (A1.27)$$

As may be inferred from the above equations, it is often the case that the uncertainties, $\delta\Delta'$ and $\delta\psi'$, achieve a minimum whenever measurements are taken near the principal angle of incidence.

The values of Δ' and ψ' are determined simultaneously at a given angle of incidence, ϕ, and wavelength, λ. Therefore, some accounting of uncertainty in ϕ and λ should be included within the total uncertainty in Δ' and ψ', $\delta\Delta'_T$ and $\delta\psi'_T$. Accordingly, one may formally write

$$\delta\psi'_T \leq \delta\psi' + \left|\frac{\delta\psi'}{\delta\phi}\right|\delta\phi + \left|\frac{\delta\psi'}{\delta\lambda}\right|\delta\lambda \qquad (A1.28)$$

and

$$\delta\Delta'_T \leq \delta\Delta' + \left|\frac{\delta\Delta'}{\delta\phi}\right|\delta\phi + \left|\frac{\delta\Delta'}{\delta\lambda}\right|\delta\lambda. \qquad (A1.29)$$

The incremental rate changes in Δ' and ψ' with respect to ϕ are determined experimentally. These are then multiplied by the uncertainty $\delta\phi$ to obtain their relative contribution to the total uncertainty in Δ' and ψ'. Because the magnitude of $\delta\lambda$ from the helium-neon laser is particularly small, the incremental changes in Δ' and ψ' with respect to λ may be considered negligible.

References

A1.1 Azzam, R.M.A., and Bashara, N.M., Ellipsometry and Polarized Light (North Holland, Amsterdam, 1987) [paperback edition].

A1.2 Aspnes, D.E., and Studna, A.A., High precision scanning ellipsometer, Applied Optics **14**, No. 1, 220-228 (1975).

Appendix 2

Formulation of the Least-Squares Problem

In order to characterize the layered structure of the sample, it is necessary to invert the standard ellipsometric equations. The equations describe how the material properties of the sample are able to induce a phase-shift in the reflected light which is then measured by the ellipsometer. Because of the complexity of the representation, it is usually not possible to find a simple analytic expression which will invert the equations. One common approach to performing such an inversion is to formulate it as a nonlinear least-squares problem [A2.1-4]. Here, one considers a sequence of forward scattering problems, where each increment of the sequence involves three distinct steps, where the steps include: starting with or providing a good estimate of values to the model parameters, determining the deviations between the experiment and model, and then updating the model parameters with better values. This sequence is continued or iterated until the magnitude of the corrections becomes sufficiently small.

The ellipsometric equation are of the form:

$$\Delta = \Delta(\phi, \lambda, \mathbf{b}) \tag{A2.1}$$

$$\psi = \psi(\phi, \lambda, \mathbf{b}), \tag{A2.2}$$

where λ is the wavelength of the incident light, ϕ is the angle of incidence, and $\mathbf{b}$ is a vector whose components specify the model parameters, e.g., indices of refraction, extinction coefficients, and thicknesses for the thin films and substrate. The standard procedure involves minimizing some non-negative scalar error expression containing the deviations between experimental and modeled values of Δ and ψ in the least-squares sense, e.g.,

$$G(\mathbf{b}) = \frac{1}{2M} \sum_{i=1}^{M} \left[\left(\Delta_i' - \Delta_i''\right)^2 + \left(\psi_i' - \psi_i''\right)^2 \right] \tag{A2.3}$$

$$= \mathbf{g}^T \mathbf{g} = |\mathbf{g}|^2, \tag{A2.4}$$

where the prime denotes the value measured by experiment, the double prime denotes the least-squares estimate, M denotes the total quantity of measurements of (Δ, ψ) from

experiment, $\mathbf{g}$ is a column vector of the deviations, i.e.,

$$g_{2i-1} = (\Delta_i' - \Delta_i'')/\sqrt{2M}, \tag{A2.5}$$

$$g_{2i} = (\psi_i' - \psi_i'')/\sqrt{2M}, \tag{A2.6}$$

where $1 \leq i \leq M$, and the superscript T denotes transposition.

The third step of the sequence is concerned with the procedure for correcting or improving the model parameters with better values, i.e., the Newton step. An estimation of the necessary correction may be realized by linearizing the functional representation of the model and solving the resulting matrix equation, $\mathbf{g}$=$\mathbf{J}\mathbf{v}$, where $\mathbf{v}$ is a vector (Newton step) for improving the model parameters that were selected to undergo variation, e.g., $v_j \sim \delta b_j$, and $\mathbf{J}$ is the sparse matrix involving the Jacobian which is not necessarily square, e.g., $J_{ij} \sim (1/\sqrt{2M})\ (\partial\Delta_i/\partial b_j)$.

Solving this matrix equation is common to optimization problems involves only linear algebra, and is well-studied. It is known that additional numerical stability or robustness may result by requiring the norm of $\mathbf{v}$ be minimized as well. This can be accomplished simply by modifying the error expression to

$$G = (\mathbf{g} - \mathbf{J}\,\mathbf{v})^T(\mathbf{g} - \mathbf{J}\,\mathbf{v}) + \kappa\mathbf{v}^T\,\mathbf{v}, \tag{A2.7}$$

where κ is a positive scalar parameter subjectively chosen to equal 0.01 for these calculations. It is also known that the columnar scaling of $\mathbf{J}$ affects the accuracy of the solution and the effectiveness of κ in moderating the rate of convergence for finding the solution $\mathbf{v}$. Here, a simple choice for the scaling can be found by using the diagonal elements from $\mathbf{J}^T\,\mathbf{J}$ and then defining the diagonal matrix, $\mathbf{S}$, where

$$S_{jj} = \sqrt{(\mathbf{J}^T\,\mathbf{J})_{jj}}\ . \tag{A2.8}$$

Then letting

$$\mathbf{J}' = \mathbf{J}\,\mathbf{S}^{-1}, \tag{A2.9}$$

$$\mathbf{v}' = \mathbf{S}\,\mathbf{v}, \tag{A2.10}$$

$$\mathbf{r} = \mathbf{g} - \mathbf{J}\,\mathbf{v} = \mathbf{g} - \mathbf{J}'\mathbf{v}', \tag{A2.11}$$

a suitable error expression may be defined by

$$G = (\mathbf{g} - \mathbf{J}'\mathbf{v}')^T(\mathbf{g} - \mathbf{J}'\mathbf{v}') + \kappa\mathbf{v}'^T\mathbf{v}'\ , \tag{A2.12}$$

$$= \mathbf{r}^T\,\mathbf{r} + \kappa\mathbf{v}'^T\mathbf{v}'\ . \tag{A2.13}$$

The criteria for critical points or relative minima is a vanishing variation, i.e., $\partial G/\partial v'_j = 0$, which yields a set of equations that may be expressed as

$$\begin{bmatrix} \mathbf{1} & \mathbf{J}' \\ \mathbf{J}'^T & -\kappa\,\mathbf{1} \end{bmatrix} \begin{bmatrix} \mathbf{r} \\ \mathbf{v}' \end{bmatrix} = \begin{bmatrix} \mathbf{g} \\ \mathbf{0} \end{bmatrix} , \qquad (A2.14)$$

that must be solved for $\mathbf{v}'$.

Because of the sparsity of the Jacobian, it is expedient to utilize an iterative method for solving the above matrix algebra problem. Algorithms [A2.5] exist that specifically address this type of problem, among which one [A2.6,7] utilizes a relatively stable Lanczos process (Krylov space decomposition) in formulating the method of steepest-descents. Essentially, the method requires that each updating vector be orthogonal to the previous update vectors. Further details may be found elsewhere [A2.6-10]. From this, one finds $\mathbf{v}'$, which then leads to $\mathbf{v}$ (the Newton step), which is then used to improve the estimate of the values for the model parameters, $\mathbf{b}$, e.g., $b_j^{\text{new}} = b_j^{\text{old}} + v_j$.

Using this improved $\mathbf{b}$, the sequence is iterated again until either: $|\mathbf{g}|$ becomes sufficiently small of the order of a few milli-degrees, i.e., the resolution of the measurement, or until $|\mathbf{v}'|$ becomes sufficiently small so that $|\mathbf{g}|$ suffers no further reduction regardless of magnitude. It is especially in this last case that it becomes necessary to scan a grid of model parameters. Multiple pseudo-minima may be encountered, e.g., non-uniqueness. Often, this serves to reveal either: (i) correlation which prevents model parameters from being resolved independently, i.e., the measurement data were not sufficiently functionally independent which thereby induces a functional dependence among the model parameters; or (ii) the inadequacy of the model in providing a sufficiently good physical description of the process, which is likely whenever $|\mathbf{g}|$ exceeds much beyond the resolution of the measurements.

Finally, it is important to realize that in the above outlined steps, the main emphasis was that of searching for and ascribing good values to the parameters of a physical model which had already been specified. It is possible that two distinct models may reduce the deviations in $|\mathbf{g}|$ to an equivalent magnitude. The problem of characterizing the sample then becomes one of comparing models and thereby selecting the better model. One heuristic approach has been to select that model which provides the smallest deviations in $|\mathbf{g}|$ while using the fewest modeling parameters and being consistent with physical reality. But a comparison assumes an ordering, and that requires a num-

ber. So the problem becomes one of reducing a model to a number. Although this reduction is certainly nontrivial, it is expedient to follow simple statistics and to consider the use of the F statistic in assessing a so-called goodness-of-fit test. For further discussion on this topic, the reader is referred to Appendix 4.

References

A2.1 Bu-Abbud, G.H., Basharaa, N.M., and Woolam, J.A., Variable Wavelength, Variable angle Ellipsometry Including a Sensitivities Correlation Test, Thin Solid Films **138**, 27-41 (1986).

A2.2 Ibrahim, M.M., and Bashara, N.M., Parameter-Correlation and Computational Considerations in Multiple-Angle Ellipsometry, J. Opt. Soc. Am. **61**, 1622-1629 (1971).

A2.3 Loescher, D.H., Detry, R.J., and Clauser, M.J., Least-Squares Analysis of the Film-Substrate Problem in Ellipsometry, J. Opt. Soc. Am., **61**, 1230-1235 (1971).

A2.4 Kim, S.Y., and Vedam, K., Proper Choice of the Error Function in Modeling Spectroellipsometric Data, Appl. Opt. **25**, 2013-2021 (1986).

A2.5 Boisvert, R.F., Howe, S.E., and Kahaner, D.K., Guide to Available Mathematical Software, Center for Applied Mathematics, National Bureau of Standards, 1984.

A2.6 Paige, C.C., and Saunders, M.A., LSQR: An Algorithm for Sparse Linear Equations and Sparse Least Squares, ACM Trans. Math. Softw. **8**, 43-71 (1982).

A2.7 Paige, C.C., and Saunders, M.A., Algorithm 583, LSQR: Sparse Linear Equations and Least Squares Problems, ACM Trans. Math. Softw. **8**, 195-209 (1982).

A2.8 Hestenes, M.R., and Stiefel, E., Methods of Conjugate Gradients for Solving Linear Systems, NBS J. Res. **49**, 409-436 (1952).

A2.9 Eisenstat, S.C., Elman, H.C., and Schultz, M.H., Variational Iterative Methods for Nonsymmetric Systems of Linear Equations, SIAM J. Numer. Anal. **20**, 345-357 (1983).

A2.10 Faber, V., and Manteuffel, T., Necessary and Sufficient Conditions for the Existence of a Conjugate Gradient Method, SIAM J. Numer. Anal. **21**, 352-362 (1984).

A2.11 Marchiando, J.F., *Semiconductor Measurement Technology:* Modeling Methods for Spectroscopic and Multiple Angle of Incidence Ellipsometry, NIST Special Publication 400-83, to be published.

Appendix 3

Sensitivity Analysis of the Model Parameters

During the calculation of the least-squares problem, the main steps center on finding accurate numerical values for the model parameters. It then follows naturally that the next logical step would involve some assessment of uncertainties associated with knowing those values. Fortunately for a restricted class of linearizable problems, one may provide estimates of the uncertainties by utilizing a formalism similar to that used in solving the least-squares problem.

Following the notation presented in Appendix 2, let the functional representation of the model be expanded to first order about the assumed fixed point, e.g.,

$$\Delta_i' - \Delta_i'' = \sum_{j=1}^{N} \left.\frac{\partial \Delta_i}{\partial b_j}\right|_o \delta b_j \; + \; \left.\frac{\partial \Delta_i}{\partial \phi}\right|_o \delta\phi, \tag{A3.1}$$

$$\psi_i' - \psi_i'' = \sum_{j=1}^{N} \left.\frac{\partial \psi_i}{\partial b_j}\right|_o \delta b_j \; + \; \left.\frac{\partial \psi_i}{\partial \phi}\right|_o \delta\phi, \tag{A3.2}$$

where N denotes the quantity of distinct model parameters, and ϕ refers to the angle of incidence. The values (b_j) and uncertainties (δb_j) of the model parameters were either determined from analyzing the measurements or taken from the literature. The literature values and associated uncertainties that are assumed known and unchanged must be considered when estimating the uncertainty in the model parameters estimated from the measurement data. This leads to a partitioning of the uncertainties δb_j into those unchanged $(\mathbf{u})$ and those varying $(\mathbf{v})$, so that the above expansion may be written as

$$\mathbf{g} = \mathbf{J}_v\,\mathbf{v} + \mathbf{J}_u\,\mathbf{u} + \mathbf{J}_\phi\tilde{\mathbf{\Phi}}, \tag{A3.3}$$

where $\mathbf{J}$ denotes the Jacobian appropriate to the partitioning, and $\tilde{\mathbf{\Phi}}$ is a columnar array involving the uncertainty $(\delta\phi_i)$ in the angle of incidence. Then, the problem of determining uncertainties in the values of the variant model parameters is that of estimating the least upper bound to $|v_j|$. A formal solution of the above equation may be expressed by

$$\mathbf{v} = \left(\mathbf{J}_v^T\mathbf{J}_v\right)^{-1}\mathbf{J}_v^T\left(\mathbf{g} - \mathbf{J}_u\,\mathbf{u} - \mathbf{J}_\phi\tilde{\mathbf{\Phi}}\right), \tag{A3.4}$$

which, of course, is contingent upon the invertibility of the square matrix, $\mathbf{J}_v^T\mathbf{J}_v$. Further, before estimating $|v_j|$, it is convenient to utilize the summing convention of repeated indices, as well as to define

$$\mathbf{D} = \left(\mathbf{J}_v^T\mathbf{J}_v\right)^{-1}\mathbf{J}_v^T. \tag{A3.5}$$

Applying absolute values signs and the triangle inequality, a strict upper bound for $|v_j|$ may be found from

$$|v_j| \leq |D_{ji}||g_i| + |D_{ji}J_{\phi,i}||\delta\phi_i| + |D_{ji}J_{u,ik}||u_k|. \tag{A3.6}$$

This representation assumes that all contributions to the uncertainty involve systematic errors, not random errors. An expression of uncertainty may be written which assumes that the contributions are treated as a combination of random and systematic errors. The total uncertainty for the j^{th} varied parameter, b_j, is estimated by

$$\sqrt{D_{ji}^2\left(s_g^2 + s_\phi^2 J_{\phi,i}^2\right)} + |D_{ji}J_{\phi,i}||\delta\phi_{sys}| + |D_{ji}J_{u,ik}||u_k|, \tag{A3.7}$$

where a summation is implied on the i index, and where the variance in the estimated deviation from the fit is

$$s_g^2 = \frac{\mathbf{g}^T\mathbf{g}}{2M - N} \tag{A3.8}$$

and the standard deviation in the angle of incidence obtained from calibration experiments of the instrument is given as

$$s_\phi = 0.002^\circ. \tag{A3.9}$$

The systematic component of uncertainty in the angle of incidence is given by $\delta\phi_{sys}$ which is set equal to $\pm 0.002^\circ$ from Table I. Equation (A3.7) was used to calculate the relative contributions to the uncertainties in the model parameters for the two-layer model reported in Table IV. The collective uncertainty for the sum of the j^{th} and k^{th} varied model parameters, $b_j + b_k$, is of the form

$$\sqrt{\left(s_g^2 + s_\phi^2 J_{\phi,i}^2\right)\left(D_{ji}^2 + D_{ki}^2 + 2D_{ji}D_{ik}\right)}$$
$$+ \left(|D_{ji}J_{\phi,i}| + |D_{ki}J_{\phi,i}|\right)|\delta\phi_{sys}|$$
$$+ \left(|D_{ji}J_{u,il}| + |D_{ki}J_{u,il}|\right)|u_l| \ . \qquad (A3.10)$$

The uncertainty in the total thickness, $t_f + t_i$, as given in Table IV, is calculated using eq. (A3.10).

Appendix 4

Goodness of Fit

A statistical procedure for testing the goodness of fit of the measurement data to a model is explained in reference [A4.1]. The procedure assumes that there are m experimental determinations of Δ and ψ for estimating the n parameters of the model and that some of these determinations represent multiple measurements taken on the same specimens over time. The repeated measurements represent the true precision of the process and are equivalent to the long-term instrumental uncertainties as explained in section V.

A sum of squares (SS) representing true precision, sometimes called a pure error term, is pooled over specimens with repetitions. Specifically, given m_i repetitions on the i^{th} specimen, the standard deviations associated with the Δ's and ψ's, denoted by $s_i(\Delta)$ and $s_i(\psi)$ with degrees of freedom $(m_i - 1)$ and $(m_i - 1)$, respectively, are pooled with standard deviations from the other specimens as follows:

$$SS_{pure\ error} = (m_1 - 1)\left(s_1^2(\Delta) + s_1^2(\psi)\right) + (m_2 - 1)\left(s_2^2(\Delta) + s_2^2(\psi)\right) + \ldots \qquad (A4.1)$$

Given the proper model, the least-squares fit to the ellipsometric measurement data will produce a sum of squares for the fit which is comparable to the pure error sum of squares. Disagreement between the two is taken as evidence that the model does not adequately describe the data. Formally, this procedure partitions the total error sum of squares into

$$SS_{total\ error} = SS_{pure\ error} + SS_{lack\ of\ fit}, \qquad (A4.2)$$

where the $SS_{total\ error}$ is defined in the usual way as the sum of squares of deviations or

$$SS_{total\ error} = \sum_{i=1}^{m} (\Delta_i' - \Delta_i'')^2 + \sum_{i=1}^{m} (\psi_i' - \psi_i'')^2, \qquad (A4.3)$$

where the measured values are denoted by primes and the predicted values are denoted

by double primes.

Then, an F statistic is constructed to test the significance of the lack-of-fit term as

$$F = \frac{[SS_{total\ error} - SS_{pure\ error}] / [df_{total\ error} - df_{pure\ error}]}{[SS_{pure\ error}] / [df_{pure\ error}]}, \qquad (A4.4)$$

where

$$df_{pure\ error} = 2(m_1 - 1) + 2(m_2 - 1) + \ldots$$

and

$$DF_{total\ error} = (2m - n).$$

The F statistic is compared with $F_\alpha(\nu_1, \nu_2)$ which represents the upper α percent point of the F distribution with ν_1 degrees of freedom in the numerator and ν_2 degrees of freedom in the denominator. If

$$F \leq F_\alpha(\nu_1, \nu_2), \qquad (A4.5)$$

there is no significant lack of fit at the α significance level.

Reference

A4.1 Draper, N., and Smith, H., *Applied Regression Analysis*, second edition (John Wiley & Sons, New York, 1981), pp. 31-38.

Appendix 5

Computer Program for Determining the Thickness of the SRM Silicon Dioxide Layer

A computer program (PROG260), which is a combination of McCrackin's FORTRAN program [A5.1] and a least-squares method for determining the SRM silicon dioxide layer thickness, is given on an accompanying 5.25-in. floppy disk. McCrackin's method is used to obtain a layer thickness and the least-squares part of the program is then used to minimize the sum of the squares of the deviations of Δ and ψ about this thickness. The disk has been formatted on an IBM PC/XT and contains the source code, object file, and executable file written using the Ryan-McFarland FORTRAN Version 2 for IBM PC/XT, AT, and compatible computers with a math coprocessor.* This program enables the user to calculate the silicon dioxide layer thickness using the values of the ellipsometric parameters Δ, ψ, and the angle of incidence, ϕ, obtained from a single ellipsometric measurement.

The program contains fixed values for the index of the medium (air) and wavelength, $\lambda = 632.8$ nm. It also contains default values for the angle of incidence, AI (degrees), refractive index of the silicon substrate, NS, refractive index of the silicon dioxide layer, NF, and an interlayer thickness (nanometers) and refractive index, INTER. The default values are as follows: AI = 70.0, NS = 3.875, 0.018, NF = 1.461, and INTER = 1.0,2.8,0.0. These default values can be modified according to the user's requirements.

For the two-layer model, the determination of the thickness of the silicon dioxide layer is based upon using the best estimates of the refractive index of the silicon dioxide layer, refractive index and thickness of the interlayer, and refractive index of the substrate. The procedure is as follows. The two-layer model data from the certificate are entered with the data entry commands, AI, NF, INTER, and NS. Entering the principal angle, ϕ, using the AI command and entering the values for Δ and ψ using the CD command will produce the thickness of the silicon dioxide layer. By adding the value reported as the interlayer thickness, 1.0 nm, as it is reported on the certificate, to the calculated thickness, $t_f + t_i$ will be obtained. The calculation for the one-layer model is performed in the same manner, but with the thickness and refractive index for the interlayer set to zero by entering the command INTER and the data "0.0." The one-layer refractive in-

dex must be entered from the certificate using NF and the appropriate value (this information can be found on page 3 of the certificate). The CD command will then produce the layer thickness for the one-layer model.

Reference

A5.1 McCrackin, F.L., A FORTRAN program for analysis of ellipsometer measurements, NBS Technical Note 479 (1969).